UNIVERSIDADE
BEIRA INTERIOR

Development of multifunctional phototherapeutic nanoagents

Inês Martins Dias da Mó

Dissertação para obtenção do Grau de Mestre em
Ciências Biomédicas
(2º ciclo de estudos)

Orientador: Prof. Doutor Ilídio Joaquim Sobreira Correia
Co-orientador: Doutor Duarte Miguel de Melo Diogo
Co-orientador: Mestre Ana Rita Lima Sousa

junho de 2020

"Success is the sum of small efforts repeated day in and day out"

- Robert Collier

Dedication

Dedico este trabalho aos meus pais, irmã e avós, por todo o apoio que me deram ao longo de todo o meu percurso académico.

Gostaria também de dedicar este trabalho a todas as pessoas que enfrentam ou enfrentaram uma doença cancerígena, em especial à minha mãe, por ter sido uma guerreira nesta luta. Espero sinceramente que a investigação nesta área continue a busca incessante de novas terapias, trazendo uma nova esperança a estas pessoas.

Acknowledgments

Em primeiro lugar, quero deixar o meu mais sincero agradecimento ao meu orientador, Professor Ilídio Correia, pela oportunidade de fazer parte do seu grupo de investigação. Agradeço todo o tempo, orientação e conselhos dados ao longo deste ano, que contribuíram para a realização desta dissertação.

Aos meus co-orientadores, Doutor Duarte Diogo e Mestre Rita Sousa, agradeço toda a dedicação, ajuda e ensinamentos que me transmitiram e que fizeram com que chegasse até aqui. Agradeço também à Mestre Cátia Alves, por todo o apoio e ajuda incondicional na realização deste projeto.

Quero também agradecer a todos os restantes elementos do grupo do Professor Ilídio, pelos momentos bem passados e ajuda ao longo desta etapa. Especialmente, aos que juntamente comigo entraram neste grupo, quero agradecer todas as conversas e todos os momentos partilhados ao longo deste ano. É um prazer poder partilhar esta etapa da minha vida com todos vocês! À minha maior parceira, a Bruna, quero agradecer toda a ajuda, amizade e por ter estado sempre presente.

À minha família, o meu suporte, não há palavras que expressem o que sinto por vocês! Um obrigado não chega para dizer o quão grata estou por todos os esforços que fizeram por mim. À minha mãe, agradeço cada chamada, cada palavra de motivação e de carinho. Ao meu pai, agradeço por todas as gargalhadas, mesmo nos dias mais difíceis, mas também todo o apoio e carinho. Um enorme obrigada às minhas avós por todos os ensinamentos passados ao longo da minha vida. À pessoa que melhor me conhece e compreende, à minha irmã gémea e futura farmacêutica, com quem partilho a vida há 22 anos, agradeço por toda a força que me deste ao longo destes 5 anos e por me dizeres sempre, “vai correr tudo bem, tu vais conseguir”. É um orgulho ter uma irmã como tu e poder partilhar a vida contigo. Obrigada!

Por fim, quero agradecer todas as amizades que fui construindo ao longo destes anos. Agradeço todas as palavras de conforto, os minutos e, às vezes horas, dispensados do vosso tempo e por todas as partilhas dos momentos bons, e dos menos bons. Todos vocês ocupam um lugar especial no meu coração.

Resumo

O cancro de mama prevalece como uma das doenças com maior taxa de mortalidade associada, um facto que pode ser explicado pela baixa eficácia e toxicidade sistémica das terapias usadas presentemente em meio clínico. Recentemente, novas abordagens terapêuticas têm sido desenvolvidas, e entre elas a terapia quimio-fototérmica mediada por nanomateriais tem revelado resultados promissores no tratamento do cancro, devido à sua capacidade para produzir um efeito anticancerígeno controlado no espaço e no tempo.

A eficácia terapêutica dos nanomateriais para a quimio-fototermia do cancro tem sido avaliada, até ao momento, usando monocamadas de células cancerígenas (modelo *in vitro* 2D). A formulação que obteve os melhores resultados *in vitro* é posteriormente testada em modelos animais portadores de tumor (modelo *in vivo*). Contudo, os modelos *in vitro* 2D não mimetizam as principais características dos tumores sólidos encontrados *in vivo*. Tal facto, faz com que determinadas nanoformulações que exibem eficácia terapêutica *in vitro*, revelem uma diminuta eficácia *in vivo*. Para ultrapassar as limitações dos modelos 2D foram desenvolvidos modelos *in vitro* 3D, conhecidos por esferóides, que têm sido usados na triagem de nanomateriais. Os esferóides são capazes de mimetizar as principais propriedades dos tumores sólidos *in vivo*, como sejam: i) a sua arquitetura 3D; ii) microambiente tumoral (os gradientes de nutrientes, pH e gases); iii) a composição celular e acelular; e iv) padrões bioquímicos e físicos de resistência às terapias.

Nesta dissertação, a eficácia anticancerígena da terapia quimio-fototérmica mediada por nanopartículas à base de albumina de soro bovino funcionalizadas com sulfobetaína metacrilato, co-encapsulando IR780 e Doxorrubicina (IR+DOX/SBMA-BSA NPs) foi avaliada em modelos *in vitro* 2D e em esferóides. Os resultados obtidos revelaram que a terapia fototérmica mediada pelas nanopartículas encapsulando IR780 (IR/SBMA-BSA NPs irradiadas com luz na região do infravermelho próximo (NIR)) reduziu a viabilidade das células para cerca de 58 %, enquanto que a quimioterapia induzida pelos nanomateriais (IR+DOX/SBMA-BSA NPs) levou a uma diminuição na viabilidade para 29 % nos modelos *in vitro* 2D. A terapia quimio-fototérmica mediada pelas nanopartículas (IR+DOX/SBMA-BSA NPs e radiação NIR) alcançou o maior efeito terapêutico, tendo reduzido a viabilidade das células cancerígenas para 1 %. Por outro lado, quando estas terapias foram avaliadas em modelos 3D de cancro de mama (esferóides), a terapia fototérmica mediada pelas nanopartículas (IR/SBMA-BSA NPs e radiação NIR) não teve um efeito citotóxico relevante para as células no interior dos esferóides, enquanto que a

quimioterapia mediada pelas nanoestruturas (IR+DOX/SBMA-BSA NPs) diminuiu a viabilidade das células presentes nos esferóides para 42 %. Por sua vez, a terapia quimio-fototérmica mediada pelos nanomateriais (IR+DOX/SBMA-BSA NPs irradiados com NIR) conseguiu reduzir a viabilidade celular no interior dos esferóides para 16 %. Estes resultados enfatizam que esta última modalidade terapêutica é a mais promissora para futura aplicação em meio clínico. Em suma, os resultados obtidos nesta dissertação demonstraram que os esferóides poderão ter um papel fundamental na triagem de nanomateriais para aplicações terapêuticas. Por outro lado, os esferóides também permitirão reduzir o número de animais usados em experimentação animal, assim como reduzir custos e acelerar o processo de desenvolvimento de novas abordagens terapêuticas.

Palavras-chave

Cancro;esferóides;nanopartículas;quimioterapia;terapia combinatória;terapia fototérmica

Resumo alargado

Atualmente, o cancro prevalece como uma das principais causas de morte em todo o mundo. Em particular, o cancro de mama continua a ser o mais diagnosticado nas mulheres e tem uma elevada taxa de mortalidade associada. Este facto deve-se às limitações das terapias usadas presentemente em meio clínico (quimioterapia e radioterapia), que para além de apresentarem uma eficácia reduzida, induzem ainda toxicidade sistémica. Deste modo, é urgente encontrar novas estratégias terapêuticas para o tratamento desta doença.

Neste contexto, a terapia quimio-fototérmica mediada por nanomateriais tem despertado junto da comunidade científica um interesse crescente. Esta modalidade terapêutica explora a capacidade que determinados nanomateriais, que encapsulam agentes fototérmicos e quimioterapêuticos, têm em se acumular de uma forma passiva no local do tumor. Após a irradiação do tumor com luz com um comprimento de onda na região do infravermelho próximo (NIR; 750-1000 nm), os nanomateriais absorvem esta radiação e promovem um aumento da temperatura local que poderá levar à morte das células cancerígenas. A utilização de luz NIR assume um papel fundamental uma vez que penetra profundamente nos tecidos e não interage significativamente com os componentes biológicos. Para além disto, o aumento de temperatura induzido pelos nanomateriais pode: i) aumentar o fluxo sanguíneo na zona do tumor, resultando numa maior acumulação de nanopartículas nessa zona; ii) permeabilizar temporariamente a membrana celular, melhorando a internalização das nanoestruturas; iii) promover o escape endossomal, conduzindo à libertação das nanoformulações no citosol; e iv) despoletar a libertação dos fármacos da matriz do nanomaterial, levando a um efeito controlado na zona do tumor. Desta forma, a ação quimio-fototérmica mediada por nanomateriais pode conduzir a um efeito terapêutico melhorado.

A eficácia terapêutica dos nanomateriais para a quimio-fototermia do cancro tem sido avaliada, até ao momento, usando monocamadas de células cancerígenas (modelo *in vitro* 2D). Posteriormente, a melhor formulação é testada em modelos animais portadores de tumor (modelo *in vivo*). Contudo, os modelos *in vitro* 2D não conseguem mimetizar as principais características dos tumores sólidos encontrados *in vivo*. Tal facto, faz com que determinadas nanoformulações que exibem eficácia terapêutica *in vitro* revelem uma baixa eficácia terapêutica *in vivo*. De forma a colmatar as limitações dos modelos 2D, os investigadores e a indústria têm apostado no desenvolvimento de modelos *in vitro* 3D, tais como esferóides, que têm sido usados na triagem de nanomateriais. A utilização destes

modelos deve-se ao facto dos esferóides serem capazes de mimetizar as principais propriedades dos tumores sólidos *in vivo*, tais como: i) a sua arquitetura 3D, ii) microambiente tumoral (os gradientes de nutrientes, pH e gases), iii) a composição celular e acelular, e iv) padrões bioquímicos e físicos de resistência às terapias.

Nesta dissertação, a eficácia anticancerígena da terapia quimio-fototérmica mediada por nanopartículas baseadas em albumina de soro bovino funcionalizadas com sulfobetaína metacrilato, co-encapsulando IR780 e Doxorrubicina (IR+DOX/SBMA-BSA NPs) foi avaliada em modelos *in vitro* 2D e em esferóides. Os resultados obtidos revelaram que as propriedades físico-químicas das SBMA-BSA NPs, preparadas através do método de nanoprecipitação, são adequadas para a sua aplicação na terapia do cancro. A terapia fototérmica mediada pelas nanopartículas encapsulando IR780 (IR/SBMA-BSA NPs e radiação NIR) reduziu a viabilidade celular para cerca de 58 %, enquanto que a quimioterapia (IR+DOX/SBMA-BSA NPs) induziu uma diminuição na viabilidade para 29 % nos modelos *in vitro* 2D. A terapia quimio-fototérmica mediada pelas nanopartículas (IR+DOX/SBMA-BSA NPs e radiação NIR) alcançou o maior efeito terapêutico, tendo reduzido a viabilidade das células cancerígenas para ~ 1 %. Por outro lado, quando estas terapias foram avaliadas em modelos 3D de cancro de mama (esferóides), a terapia fototérmica mediada pelas nanopartículas (IR/SBMA-BSA NPs e radiação NIR) não teve um efeito citotóxico relevante para as células no interior dos esferóides, enquanto que a quimioterapia mediada pelas nanopartículas (IR+DOX/SBMA-BSA NPs) diminuiu a viabilidade celular nos esferóides para 42 %. Por fim, a terapia quimio-fototérmica mediada pelas nanoestruturas (IR+DOX/SBMA-BSA NPs irradiadas com NIR) conseguiu reduzir a viabilidade dos esferóides para 16 %. Estes resultados enfatizam que esta última modalidade terapêutica é a mais promissora. Em suma, os resultados obtidos nesta dissertação demonstraram que os esferóides poderão ter um papel fundamental na triagem de nanomateriais para aplicações terapêuticas. Por outro lado, os esferóides também permitirão reduzir o número de animais usados em experimentação animal, assim como diminuir os custos e acelerar o processo de desenvolvimento de novas abordagens terapêuticas.

Abstract

Breast cancer remains as one of the world's deadliest diseases, a fact that can be explained by the low efficacy and systemic toxicity of the therapies currently in use in the clinic. Recently, researchers have been developing new therapeutic approaches, among which the chemo-photothermal therapy mediated by nanomaterials has been showing promising results, due to its capacity to produce a spatio-temporal controlled anti-cancer effect.

During the development of nanomaterials aimed for cancer chemo-photothermal therapy, their efficacy is initially assessed using monolayers of cancer cells (2D *in vitro* models). The best formulations screened in 2D are then evaluated in tumor bearing mice (*in vivo* models). However, the 2D *in vitro* models present some drawbacks, since they are unable to mimic the key features of the *in vivo* solid tumors. Due to this reason, several nanoformulations that displayed therapeutic efficacy when tested in the 2D *in vitro* models induce a subpar effect *in vivo*. To overcome this limitation, spheroids (3D *in vitro* models) have recently emerged for the screening of nanomedicines. In fact, spheroids are able to reproduce the main properties of the *in vivo* solid tumors, namely: i) their 3D architecture, ii) microenvironment (gradients of nutrients, pH and gases), iii) cellular and acellular composition, and iv) biochemical and physical resistance patterns to the therapeutics.

In this Master thesis, the efficacy of the chemo-photothermal therapy mediated by nanoparticles based on bovine serum albumin functionalized with sulfobetaine methacrylate, co-encapsulating IR780 and Doxorubicin (IR+DOX/SBMA-BSA NPs) was evaluated in 2D *in vitro* models and spheroids. In 2D *in vitro* models, it was found that photothermal therapy mediated by nanoparticles loading IR780 (IR/SBMA-BSA NPs and NIR irradiation) reduced cells' viability to about 58 %, while chemotherapy induced by nanomaterials (IR+DOX/SBMA-BSA NPs) led to a decrease in their viability to 29 %. In addition, the nanoparticles' mediated chemo-photothermal therapy (IR+DOX/SBMA-BSA NPs and NIR irradiation) achieved a better therapeutic effect by reducing cells' viability to 1 %. On the other hand, when the therapies were screened on 3D breast cancer models (spheroids), the photothermal therapy mediated by the nanoparticles (IR/SBMA-BSA NPs and NIR irradiation) did not induce an appreciable cytotoxic effect, while the chemotherapy mediated by the nanostructures (IR+DOX/SBMA-BSA NPs) decreased the viability of the spheroids to 42 %. In turn, the chemo-photothermal therapy mediated by the nanomaterials (IR+DOX/SBMA-BSA NPs and NIR irradiation) was able to further reduce the viability of spheroids to 16 %, revealing that this is the most promising therapeutic modality.

Overall, the results obtained in this dissertation highlight the importance of the use of spheroids in the screening of the nanomedicines' therapeutic capacity. In addition, spheroids may also speed-up the therapeutics' development process, as well as contribute to decrease the number of animals used in experimentation.

Keywords

Cancer, chemotherapy, combinatorial therapy, nanoparticles, photothermal therapy, spheroids.

List of Publications

Articles published in international peer reviewed journals:

Mó, I.*, Sabino, I. J.*, de Melo-Diogo, D.*, Lima-Sousa, R., Alves, C. G., Correia, I. J.; *The importance of spheroids in analyzing nanomedicines' efficacy*, Nanomedicine, 2020, *in press* (DOI: 10.2217/nnm-2020-0054).

* These authors contributed equally to this article

Articles submitted for publication in international peer reviewed journals:

Mó, I., Alves, C. G., de Melo-Diogo, D., Lima-Sousa, R., Correia, I. J.*; Assessing the combinatorial chemo-photothermal therapy mediated by sulfobetaine methacrylate-functionalized nanoparticles in 2D and 3D in vitro cancer models*.

Index

Figure Index

List of Abbreviations

ANOVA	Analysis of variance
BSA	Bovine Serum Albumin
Chemo-PTT	Chemo-Photothermal Therapy
DLS	Dynamic Light Scattering
DMEM-F12	Dulbecco's Modified Eagle Medium-F12
DOX	Doxorubicin
DTT	DL-Dithiothreitol
DTX	Docetaxel
ECM	Extracellular Matrix
EPR	Enhanced Permeability and Retention
FBS	Fetal Bovine Serum
FTIR	Fourier Transform Infrared Spectroscopy
HSP70	Heat Shock Protein 70
ICG	Indocyanine Green
IR/SBMA-BSA NPs	IR780 loaded SBMA-BSA Nanoparticles
IR+DOX/SBMA-BSA NPs	IR780 and DOX loaded SBMA-BSA Nanoparticles
MCF-7	Michigan Cancer Foundation-7
NHDF	Normal Human Dermal Fibroblasts
NIR	Near Infrared
ns	Non-significant
PBS	Phosphate Buffered Saline
PDI	Polydispersity Index
PEG	Poly(ethylene glycol)
P-gp	P-glycoprotein
PLGA	Poly (lactic-*co*-glycolic) acid
PTT	Photothermal Therapy
ROS	Reactive Oxygen Species
SBMA	[2-(Methacryloyloxy) ethyl] dimethyl-(3- sulfopropyl) ammonium hydroxide
SBMA-*g*-BSA	BSA grafted with SBMA
S.D.	Standard Deviation
TEM	Transmission Electron Microscopy

Chapter 1

Introduction

Part of the subsection “1.3. *In vitro* models used to evaluate cancer combinatorial therapy mediated by nanomaterials” of this chapter is based on the publication entitled: “The importance of spheroids in analyzing nanomedicines' efficacy”, Nanomedicine, 2020, *in press* (DOI: 10.2217/nnm-2020-0054).

1. Introduction

1.1. Cancer development and hallmarks

1.1.1. Cancer

Cancer remains as a serious public health problem, since it has associated high rates of incidence and mortality. For 2020, it was estimated that 1 806 590 new cases of cancer will be diagnosed and 606 520 of deaths may occur as a consequence of this disease, just in the United States of America [1]. In Portugal, the data available from the Portuguese National Health Service indicates that around 50 000 new cases of cancer are diagnosed *per* year, with the incidence of this disease growing at a rate of 3 % *per* year [2].

The cancer development process (carcinogenesis) involves three stages that occur slowly, and in which cells suffer several genetic and epigenetic changes (Figure 1) [3, 4].

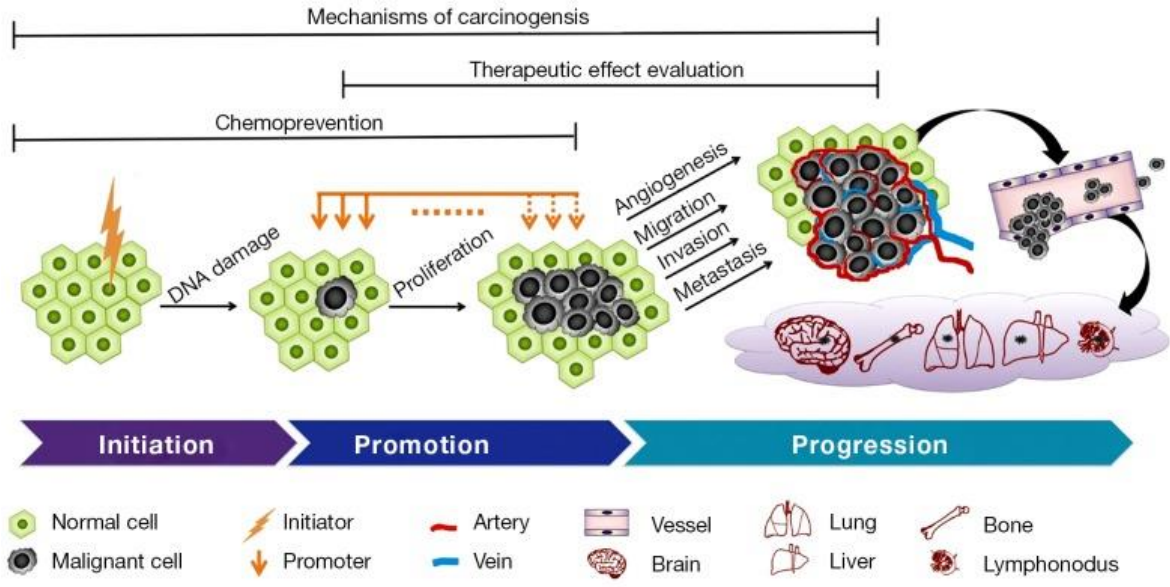

Figure 1: Schematic representation of the different stages of the carcinogenesis process. The first stage is the initiation, in which cells are exposed to mutagens/initiators that induce changes in cells' genetic material. Promotion is the second stage and it is characterized by the appearance of benign tumors. The last stage is known as progression and it is characterized by an exaggerated proliferation of the altered cells that lead to the formation of malignant tumors, and even to the appearance of metastasis (Adapted from [4]).

These stages are: i) initiation, that occurs when cells are exposure to mutagens/initiators and result in irreversible alterations in their genetic material, ii) promotion, which involves the action of promoters that induce the proliferation of initiated cells, leading to an increase in the number of cells in a specific region of the body, forming a benign tumor, and

iii) progression, that is characterized by changes in the karyotype that lead to an uncontrolled and irreversible replication of transformed cells, resulting in the transformation of a benign tumor into a malignant tumor (Figure 1) [3, 4].

According to Hanahan and Weinberg, malignant cells display six hallmarks (Figure 2): i) maintenance of proliferative signaling, ii) unmanageable angiogenesis, iii) avoidance of tumor suppressor genes, iv) resistance to cell death mechanisms, v) limitlessly replication, and vi) invasive capacity [5].

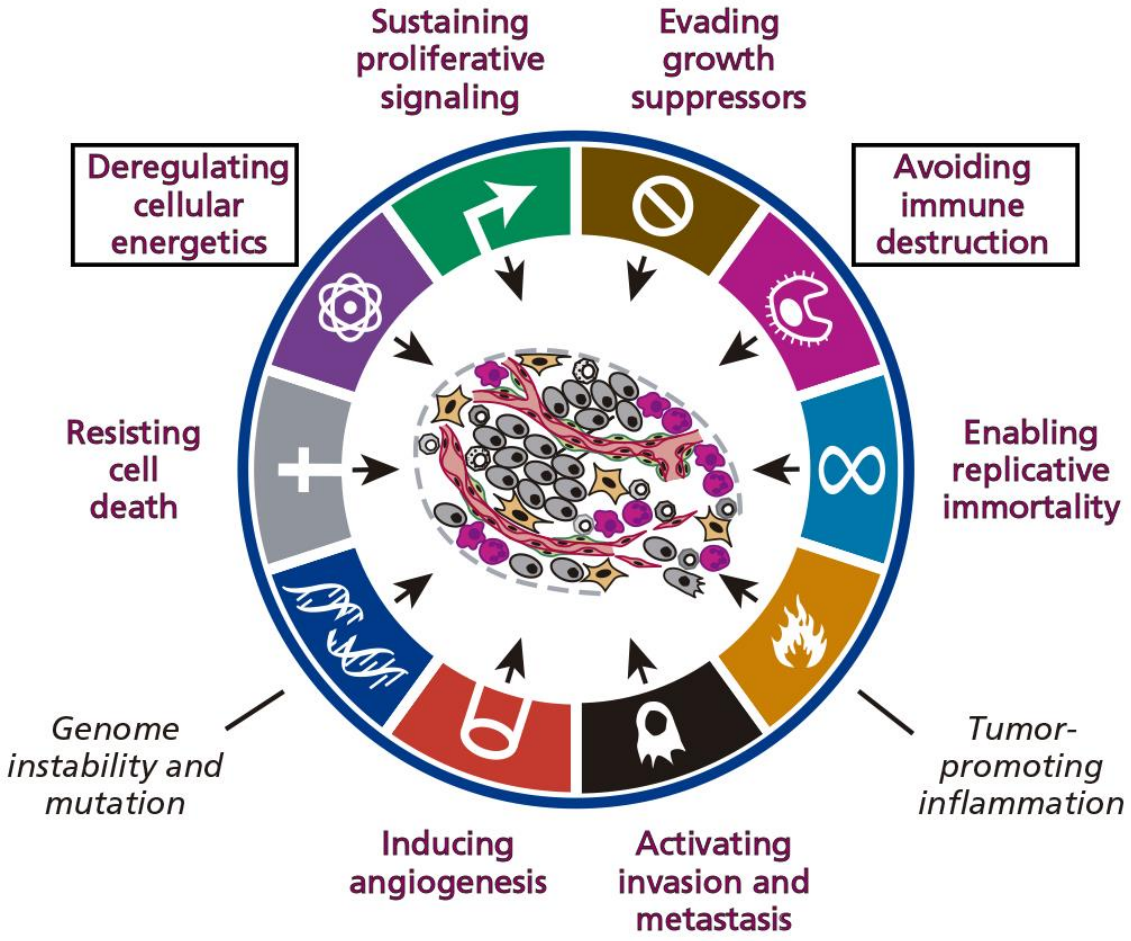

Figure 2: The cancer hallmarks described by Hanahan and Weinberg. The first six hallmarks proposed in 2000 are: i) maintenance of proliferative signaling, ii) unmanageable angiogenesis, iii) avoidance of tumor suppressor genes, iv) resistance to cell death mechanisms, v) limitlessly replication, and vi) invasive capacity. In 2011, two new hallmarks were added: vii) deregulating cellular energetics and viii) capacity to avoid destruction by the immune system. The two facilitator characteristics of the hallmarks' acquisition are: genome instability and mutation and tumor-promoting inflammation (Adapted from [6]).

Through autocrine signaling, cancer cells are able to produce growth factors that promote their proliferation [5]. Additionally, cancer cells are in constant interaction with stromal

cells, and through these communications, cancer stromal cells are stimulated to secrete growth factors, which enhance cancer cells proliferation [5, 7, 8].

The changes that occur in the transformation of a healthy cell into a malignant cell are triggered by mutations, which can occur in oncogenes (*e.g.* RAS and HER2) or in tumor suppressor genes (*e.g.* p53, BRCA1 and BRCA2) [3-5]. For instance, mutations that occur in tumor suppressor gene p53 are responsible for cells' resistance to apoptosis [9]. In addition, cancer cells also acquire resistance to cell death due to the high expression of anti-apoptotic proteins (*e.g.* Bcl-2, Bcl-x_L, Bcl-w) and/or low expression of pro-apoptotic proteins (*e.g.* Bax and Bak) [5, 9].

Additionally, the cancer cells capacity to proliferate indefinitely is acquired through the overexpression of telomerase [5]. This enzyme is responsible for the maintenance of the length of telomeres, by adding telomeric segments to the ends of chromosomes. Such process protects telomeres from degradation and/or end-to-end fusion and, consequently, avoid cell senescence [5, 10]. In this way, cancer cells are able to continuously proliferate, acquiring immortality [5, 10].

The growth of a tumor requires the presence of a vasculature that provides malignant cells access to nutrients and oxygen, as well as allows the elimination of metabolites and carbon dioxide [5]. In this way, the angiogenesis occurring in the malignant tissue is fundamental to support the tumor growth [5]. The new vasculature is characterized by a disorganized 3D architecture with fenestrations that allow cancer cells to leak through and, consequently, spread to other sites, forming micrometastasis that may evolve to large tumors [5, 11]. This escape of cancer cells to other tissues is due to the down regulation of the expression of cell-cell adhesion proteins (*e.g.* E-cadherin) and due to an increased expression of mesenchymal markers (*e.g.* N-cadherin), which are associated with cell migration [5, 12].

A decade later, these researchers introduced two more cancer hallmarks. The first is the deregulation of cellular energetics by cancer cells in order to support their development [5, 6]. The metabolism of cancer cells is generally referred to as "aerobic glycolysis" [5]. In this metabolic pathway, cancer cells obtain energy through the conversion of pyruvate to lactate, even in the presence of oxygen, leading their growth in an uncontrolled manner [5]. In addition, the reprogramming of energy metabolism of cancer cells is associated with oncogenes (*e.g.* RAS and MYC) and the activity loss of tumor suppressor genes (*e.g.* p53) [6]. The second new hallmark is the capacity of malignant cells to avoid destruction by the immune system [5, 6]. The immune system plays a very important role in preventing the progression of tumors [5]. Thus, any functional change that occurs in the components of the

immune system (*e.g.* T and B lymphocytes, macrophages and natural killer cells), leads to an increased probability of developing cancer [5, 6]. In addition, when the host's immune system is immunocompetent, the immunogenic cancer cells are eliminated. Immunocompromised patients are unable to perform such elimination and cancer cells continue to proliferate [5].

1.1.2. Breast Cancer

Breast cancer is among the top 3 types of cancer diagnosed in women, being the second leading cause of death in females [1]. For the year 2020, it is estimated that 276 480 new cases and 42 170 deaths will occur just in the United States of America [1]. In the case of Portugal, the data available from the *Liga Portuguesa Contra o Cancro* estimates that in the portuguese female population, 11 new cases and 4 deaths related to breast cancer are registered daily [13].

Breast cancer is a heterogeneous disease, having associated diverse risk factors, such as: age (the incidence is higher in women over the age of 50 [1]), family history (the risk is greater in families whose members had breast cancer [14]) and genetic predisposition (associated with mutations that occur in the BRCA1 and BRCA2 genes [14]). Moreover, there are a number of lifestyle-related factors that can increase the probability of developing breast cancer, namely: smoking, alcohol consumption, unhealthy diet and lack of physical activity [14-16].

Healthy breast ducts are mainly composed by two types of cells (luminal epithelial cells and myoepithelial cells) which form the inner layer and outer layer of these structures, respectively, and a basement membrane that is surrounded by the myoepithelial cells [17, 18]. Moreover, other components of the stroma, such as fibroblasts, myofibroblasts, endothelial and immune cells are also present in healthy ducts [18, 19]. Breast cancer begins with an excessive proliferation of epithelial cells due to genetic and epigenetic changes, that consequently lead to the appearance of an *in situ* carcinoma (Figure 3) [18, 19]. In addition, these changes will induce an increase in stromal cells and infiltrated leukocytes, a decrease in the myoepithelial cells and the degradation of the basement membrane [18, 19]. These changes and an increase in the secretion of growth factors, as well as cytokines, chemokines and matrix metalloproteinases, promote the continuous proliferation of malignant cells (Figure 3) [19].

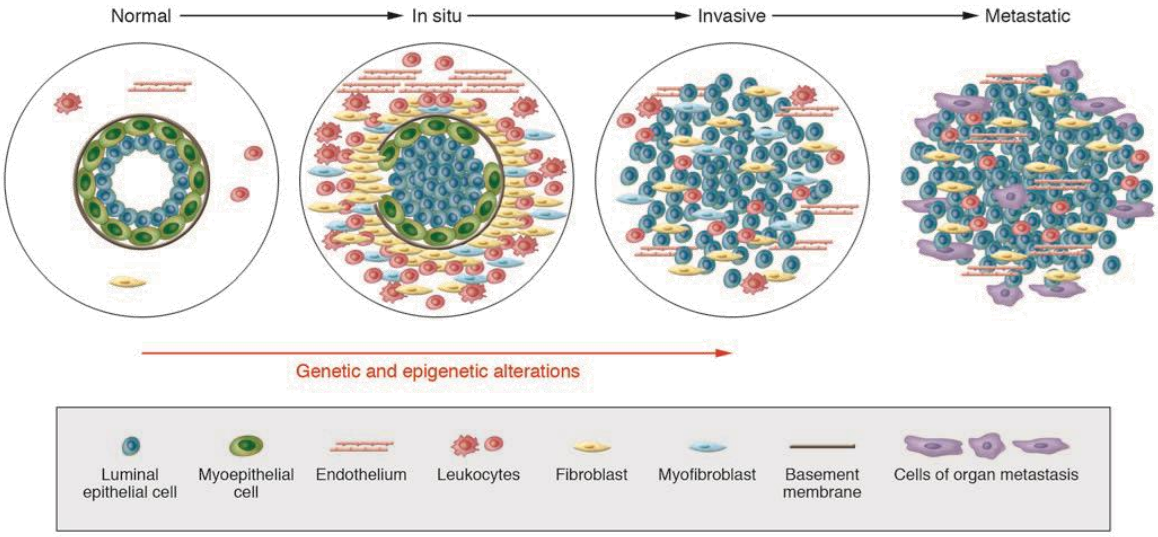

Figure 3: Schematic representation of the process of breast cancer development. The epithelial cells of the mammary ducts undergo genetic and epigenetic changes that culminate in the appearance of breast cancer cells. These changes will induce an increase in stromal cells and infiltrated leukocytes, a decrease in the myoepithelial cells and the degradation of the basement membrane, forming an *in situ* carcinoma. The *in situ* carcinoma evolves to an invasive carcinoma due to the complete loss of myoepithelial cells and degradation of the basement membrane (Adapted from [18]).

The *in situ* carcinoma can evolve into an invasive state due to the complete loss of myoepithelial cells and degradation of the basement membrane (Figure 3) [18, 19]. Consequently, the malignant cells can spread to other tissues, originating metastasis [18, 19]. Additionally, breast cancer cells can interact with cancer-associated fibroblasts which are responsible for providing cancer cells invasive, angiogenic and metastatic capacities [19, 20]. On the other hand, tumor-associated macrophages also interact with breast cancer cells by secreting cytokines, chemokines and growth factors that support angiogenesis and cancer cells invasion/metastization [19, 20].

The most common treatments used for breast cancer therapy are surgery (tumor removal in non-metastatic states), chemotherapy and radiotherapy (administration of drugs and high-energy radiation, respectively) [21, 22]. However, these treatments induce notorious side effects, due to their reduced selectivity, affecting the patients' quality of life [22]. Cancer cells can also develop resistance to chemotherapy and radiotherapy, further reducing the effectiveness of these therapeutic modalities [22, 23]. In this way, there is an urgent need to develop new and more effective therapies to treat breast cancer and thus counteract the alarming numbers associated with this disease.

1.2. Combinatorial therapy mediated by nanomaterials

1.2.1. Overview of cancer combinatorial therapy mediated by nanomaterials

The sole application of conventional cancer therapies, such as chemotherapy, is associated with several drawbacks, such as: reduced stability of the chemotherapeutic agents and low selectivity towards cancer cells [24, 25]. Additionally, cancer cells may also develop multiple drug resistance mechanisms. For instance, the overexpression of the P-glycoprotein efflux pump (P-gp) prevents anticancer drugs from exerting their effect [25]. On the other hand, malignant cells' resistance towards radiotherapy is associated with the presence of cancer stem cells [26].

To surpass this lack of efficacy, combinatorial therapy appears to be a promising strategy to treat cancer [27, 28]. This modality explores possible synergistic effects, lowering the dose of therapeutics, and overcoming drug resistance mechanisms [27, 28]. However, these synergistic interactions may also produce an escalation of the side effects [24, 28, 29].

The development of nanocarriers has emerged as a promising approach to improve the selectivity of combinatorial therapies, allowing a spatio-temporal controlled effect with lower side effects [24, 29, 30]. Nanoparticles are usually administered through intravenous administration, and, due to their specific set of properties, may accumulate at the tumor site [31]. Generally, nanomaterials with a size between 50 and 200 nm can leak through the abnormal tumor vasculature (vessels with fenestraes between 200-1200 nm) and become confined at the tumor site (tumor tissue has an impair lymphatic drainage) – known as the Enhanced Permeability and Retention (EPR) effect, while avoiding at the same time clearance by the kidneys and uptake by the liver/spleen [32, 33].

Besides the nanoparticles' size, their charge is also decisive since it influences their opsonization during circulation, interaction with the tumors' extracellular matrix (ECM) and uptake by cancer cells [32]. In this regard, the so called neutrally charged nanomaterials, which have a surface charge between -10 and +10 mV, are considered ideal [34]. The surface composition of the nanomaterials is also crucial in their biological fate [32]. In this regard, the functionalization of nanomaterials' surface with hydrophilic coatings (*e.g.* poly(ethylene glycol) (PEG) [35], poly(oxazolines) [36], zwitterionic brushes [37]) can enhance their blood circulation time, favouring their accumulation in the tumor zone [35-37].

Finally, the surface of the nanoparticles can be decorated with targeting agents (*e.g.* folic acid, transferrin, anti-CD44 antibodies, etc.), that bind to receptors overexpressed by cancer cells, thus improving their selectivity [31]. In this way, nanoparticles can increase the half-life of the encapsulated agents and improve their tumor accumulation while decreasing their off-target toxicity [24, 30].

Several reports have shown that the combinatorial therapies mediated by nanomaterials, such as: chemo-chemotherapy [38], chemo-gene delivery [39] and chemo-phototherapies [40] are more effective than their respective single therapies [38, 40-43].

The therapeutic efficacy of the combinatorial chemo-chemotherapy mediated by nanocarriers has been demonstrated in several studies [38, 41, 44, 45]. For instance, Liu *et al.* demonstrated that nanocarriers co-encapsulating Doxorubicin (DOX) and Docetaxel (DTX) can decrease cancer cells' viability to about 15 % [38]. In this same study, the use of nanocarriers loaded with only DOX or DTX (single therapies), just diminished cancer cells' viability to about 25 % and 30 %, respectively [38].

Nanocarriers have also been used for the co-administration of chemotherapeutics and genetic material (*e.g.* siRNA) [39, 43, 46]. This type of therapy aims to silence or re-establish specific proteins with the intent of improving the efficacy of the drugs [39, 43, 46]. Meng *et al.* verified that nanoparticles encapsulating DOX and siRNA targeting P-gp (a major DOX efflux pump) were able to supress the expression of P-gp, leading to an increased intracellular accumulation of DOX [39].

More recently, the use of chemo-photothermal therapy (chemo-PTT) mediated by nanomaterials has been revealing promising results, which attracted the attention of researchers (described in the following section).

1.2.2. Combinatorial chemo-PTT mediated by nanomaterials

The use of PTT mediated by nanomaterials for the treatment of cancer has been demonstrating a great potential [32, 47, 48]. In general, this therapeutic approach employs inorganic materials with Near Infrared (NIR) absorption (*e.g.* graphene derivatives [49], gold nanorods [50], transition metal dichalcogenides [51]) or organic NIR dyes encapsulated in nanostructures (*e.g.* Indocyanine Green (ICG) [52], IR780 [37], IR808 [53], IR820 [54], IR825 [55]). In this modality, after the nanomaterials reach the tumor site, this zone is irradiated with NIR light [32]. Then, the photothermal agents absorb this radiation and convert it into heat, inducing damage on the cancer cells [32, 56].

The use of NIR light is crucial due to its low interaction with biological components (*e.g.* water, hemoglobin, melanin) and its high deep penetration into tissues (1-2 cm [57]) (Figure 4) [32, 58].

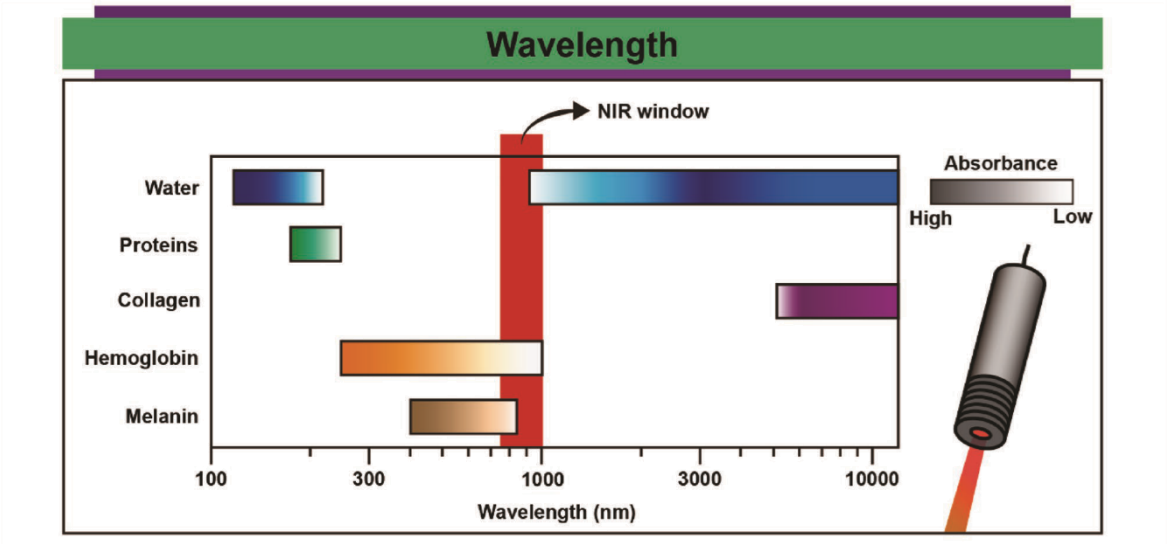

Figure 4: Schematic representation of the absorption of different biological components in the NIR wavelength range (750-1000 nm). In this wavelength range, water, proteins, collagen, hemoglobin and melanin have poor/minimal absorption. In this way, the NIR light can achieve a deep penetration into tissues, reaching the tumor-homed nanomaterials without affecting significantly other biological components (Adapted from [32]).

Furthermore, the temperature increase mediated by nanomaterials can augment the blood circulation into the tumor site, increasing the number of tumor-homed nanoparticles [58]. The attained temperature increase can also affect the permeability of the cells' membrane, enabling a better internalization of the nanomaterials (Figure 5) [58, 59]. Compared to other therapies, nanomaterials mediated PTT has the ability to produce an on-demand effect with reduced side effects [49, 60].

However, the heterogeneous heat distribution that results from the isolated application of PTT mediated by nanomaterials may prevent the total eradication of the tumor [61-64]. In this way, nanomaterials' incorporating NIR agents can also be loaded with chemotherapeutic agents, improving the efficiency of both therapies [36, 40, 42, 62]. In this regard, the nanomaterials' photoinduced heat can promote the rupture of the endosomes and trigger the release of the drugs from the nanomaterial, allowing them to reach the cells' cytoplasm (Figure 5) [58, 59]. Therefore, the combinatorial chemo-PTT mediated by nanomaterials can induce a therapeutic effect that surpasses the efficacy of the nanomaterials' mediated single therapies [64-66].

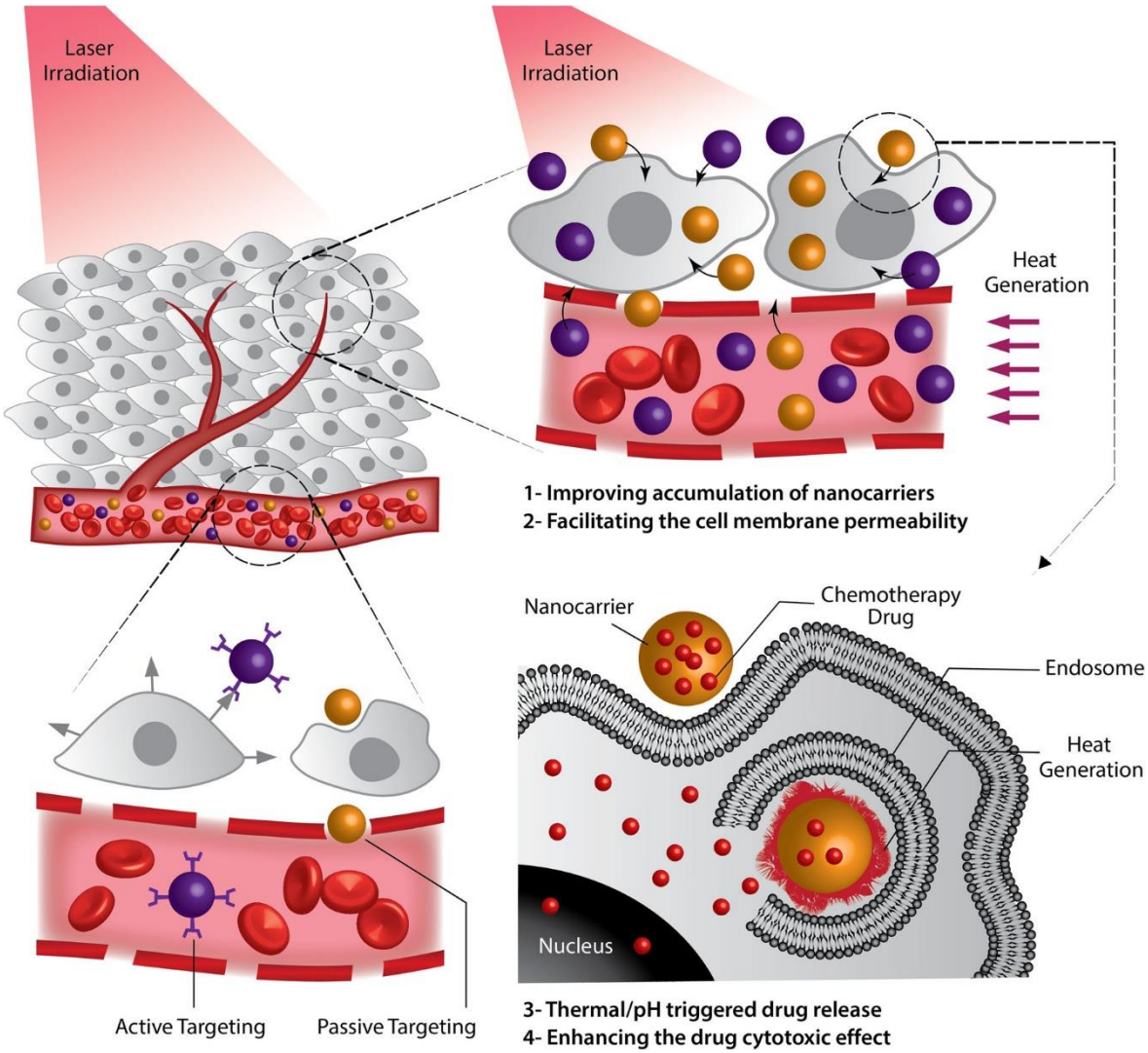

Figure 5: Schematic representation of the combinatorial chemo-PTT mediated by nanomaterials. First, nanomaterials are administered intravenously and accumulate at the tumor site through the EPR effect. Then, the tumor site is externally irradiated with NIR light, which leads to a temperature increase that can: 1) increase the blood flow into the tumor microenvironment and thus enhance the amount of tumor-homed nanoparticles, 2) increase the permeability of the cells' membrane, improving the nanoparticles uptake, 3) trigger the endosomal escape of the nanoparticles or 4) improve the chemotherapeutics' toxicity by triggering their controlled release in the cytoplasm (Adapted from [59]).

Several studies have investigated the therapeutic effect of combinatorial chemo-PTT mediated by nanomaterials [36, 62, 65, 67, 68]. Chen *et al.* verified that PEG-functionalized reduced graphene oxide loaded with resveratrol could increase the intracellular content of resveratrol, from about 3 % to 30 %, upon exposure to NIR light for 10 min (808 nm, 0.6 W cm^{-2}) [67]. De Melo-Diogo *et al.* demonstrated that the combination of poly(oxazoline)-functionalized graphene oxide co-loaded with DOX and D-α-Tocopherol succinate with NIR light (808 nm, 1.7 W cm^{-2}, 5 min) could decrease the cancer cells' viability to about 39 % [36]. In contrast, the nanomaterials' mediated chemotherapy

(DOX and D-α-Tocopherol succinate loaded functionalized graphene oxide) only reduced cells' viability to about 61 %, while the nanomaterials' mediated PTT (functionalized graphene oxide and NIR light) was unable to induce a therapeutic effect [36].

In another work, Zheng *et al.* developed poly (lactic-*co*-glycolic acid) (PLGA)-lecithin-PEG nanoparticles co-loaded with ICG and DOX (5.50 μg mL^{-1} of ICG and 6.00 μg mL^{-1} of DOX) [68]. The use of this nanoformulation combined with NIR radiation (808 nm, 1.6 W cm^{-2}, 5 min) reduced DOX-resistant cancer cells' viability to 5 % (combinatorial chemo-PTT). At the same concentration of ICG and DOX, the sole application of PTT (nanoparticles encapsulating ICG and NIR light) and chemotherapy (nanoparticles encapsulating DOX) only led to a reduction in the cells' viability to 31 % and 66 %, respectively [68]. In another study, Li *et al.* showed that micelles formulated with IR780 and DOX (2.60 μg mL^{-1} of IR780 and 6.00 μg mL^{-1} of DOX) reduced the cells' viability to 24 % when exposed to NIR light (808 nm, 1.5 W cm^{-2}, 5 min) [69]. On the other hand, these micelles encapsulating only IR780 and exposed to NIR light (nanomaterials' mediated PTT) only reduced cells' viability to 59 %, while the micelles only formulated with DOX (nanomaterials' mediated chemotherapy) just decreased the viability of cells to 89 % [69].

Among the different types of chemo-photothermal nanoagents developed so far, those incorporating IR780 have been showing the most promising results (described in the next section).

1.2.3. Nanomaterials incorporating IR780 for cancer chemo-PTT

Nanomaterials co-encapsulating IR780 (a hydrophobic heptamethine cyanine dye with NIR absorption [70]) and chemotherapeutics have been showing promising results for cancer chemo-PTT [40, 62, 64, 66, 69, 71]. The encapsulation of IR780 in nanomaterials is crucial since it improves its solubility and cytocompatibility, enabling its use in cancer therapy [31, 71-73].

Compared to other inorganic-based nanosystems (*e.g.* graphene derivatives, gold nanorods) used for chemo-PTT, the formulation of nanoparticles co-encapsulating IR780 and drugs is a straightforward process since it only requires the usage of nanomaterials with a hydrophobic core (*e.g.* PLGA nanoparticles, PEG-based micelles, bovine serum albumin (BSA)-based nanocarriers) [64, 65, 74, 75]. Furthermore, IR780-incorporating nanomaterials have optical properties superior to those incorporating other NIR-responsive dyes (*e.g.* ICG, IR820) [70].

In general, nanomaterials incorporating IR780 and chemotherapeutics can achieve a suitable therapeutic effect by: i) using lower drug doses, ii) lower NIR exposure times, and/or iii) weaker radiation intensities [31, 70]. In this way, the chemo-PTT mediated by nanomaterials co-encapsulating IR780 and chemotherapeutics can achieve a greater therapeutic outcome. For instance, Alves *et al.* produced nanoparticles functionalized with Hyaluronic acid co-loaded with IR780 and DOX (3.50 μg mL^{-1} of IR780; 1.93 μg mL^{-1} of DOX), verifying that upon irradiation with NIR light (808 nm, 1.7 W cm^{-2}, 5 min), these could reduce cancer cells' viability to 20 % [40]. In contrast, the same formulation containing only IR780 and exposed to NIR radiation (nanomaterials' mediated PTT) only reduced the viability of cancer cells to 59 % [40]. In another study, Yang *et al.* showed that polymeric nanoparticles, co-loaded with IR780 and DTX (68.00 μg mL^{-1} of IR780 and 20.00 μg mL^{-1} of DTX), exposed to NIR radiation (808 nm, 1.5 W cm^{-2}, 5 min) could produce a greater therapeutic effect against breast cancer cells when compared to the standalone nanomaterials' mediated chemotherapy or PTT [66]. Yan *et al.* demonstrated that the chemo-PTT mediated by liposomes co-loaded with IR780 and DOX induced complete tumor eradication *in vivo* (808 nm, 1 W cm^{-2}, 5 min) [62]. On the other hand, the sole action of nanomaterials' mediated PTT (liposomes loaded with IR780 and NIR light) or chemotherapy (liposomes loaded with DOX) only induced a reduction of the tumor growth [62].

Before their potential clinical application, the efficacy of the chemo-PTT mediated by nanomaterials incorporating IR780 and chemotherapeutics must be extensively investigated using *in vitro* and *in vivo* cancer models (reviewed in the next section).

1.3. *In vitro* models used to evaluate cancer combinatorial therapy mediated by nanomaterials

Classically, the development of nanomaterials aimed for cancer chemo-PTT employs two pre-clinical efficacy testing stages: *in vitro* assays using monolayers of cancer cells and *in vivo* assays using tumor-bearing mice.

Monolayers of cancer cells (2D models) are the most commonly employed *in vitro* model to screen the efficacy of the nanomaterials [36, 40, 64, 76]. In these 2D *in vitro* cancer models, the cells are seeded on flat, rigid substrates, usually made of polystyrene (*e.g.* culture flasks (T-Flasks or Petri dishes)), growing in monolayers [77-79]. The main advantages of this type of model are its low cost, simplicity, ease of preparation/maintenance and reproducibility [78, 79]. After screening therapies mediated by nanomaterials in the monolayers, the best

candidates are selected for posterior evaluation in *in vivo* assays [62, 76, 80].

However, 2D *in vitro* models are unable to reproduce the 3D organization/architecture of the *in vivo* tumors [78]. For instance, the 2D models also lack cell-cell and cell-ECM interactions, which are extremely important for several cell functions, such as cellular differentiation and proliferation [78, 79]. Due to the poor correlation between the features of the 2D *in vitro* models and the *in vivo* tumors, the therapeutic efficacy of nanoformulations in 2D models is often not reproduced in *in vivo* models [81-84]. For example, the chemo-PTT mediated by PEGylated dendrimer-DOX-gold nanorods conjugates, reduced the viability of cancer monolayers to about 2 %, while *in vivo* only caused a reduction of the tumor growth [84]. In another study, the chemo-PTT mediated by nanoparticles functionalized with polydopamine (PTT agent) and loaded with DOX, reduced the viability of malignant cells to about 9 %, while *in vivo* only caused tumor regression [83].

To overcome this problem in the pre-clinical *in vitro* testing stage, the efficacy of nanomaterials has started to be screened in 3D *in vitro* cancer models [40, 85-87]. In these emerging cancer models, cells can be seeded in artificial 3D matrices (*e.g.* inserts, structures of hydrogel and sponges), originating the scaffold-based 3D cultures [78, 88]. In turn, the non-scaffold-based 3D cultures (spheroids) are originated by the aggregation of cells using different techniques [78, 89, 90]. For example, the liquid overlay technique uses non-adhesive surfaces to form spheroids on its surface, and the hanging drop technique comprises the formation of cellular aggregates within droplets suspended on a hydrophobic surface [89]. Cellular aggregates can also be formed by the forces of fluid flow in devices with microchannels (microfluidic chips) or in spinning flasks, where the cells are subject to a constant circular rotation (spinning rotation) [77, 78, 89].

Recently, the ability of spheroids to reproduce numerous properties of the *in vivo* solid tumors has promoted their use for the pre-clinical testing of nanoparticles [40, 85, 86]. Large spheroids (> 500 μm) are cellular aggregates that can mimic the solid tumors' 3D structure, cell-cell and cell-ECM interactions, as well as the gradients of oxygen, pH and nutrients – Figure 6. Due to these features, spheroids display a resistance to therapeutics quite similar to that occurring in solid tumors [78, 87, 89, 91].

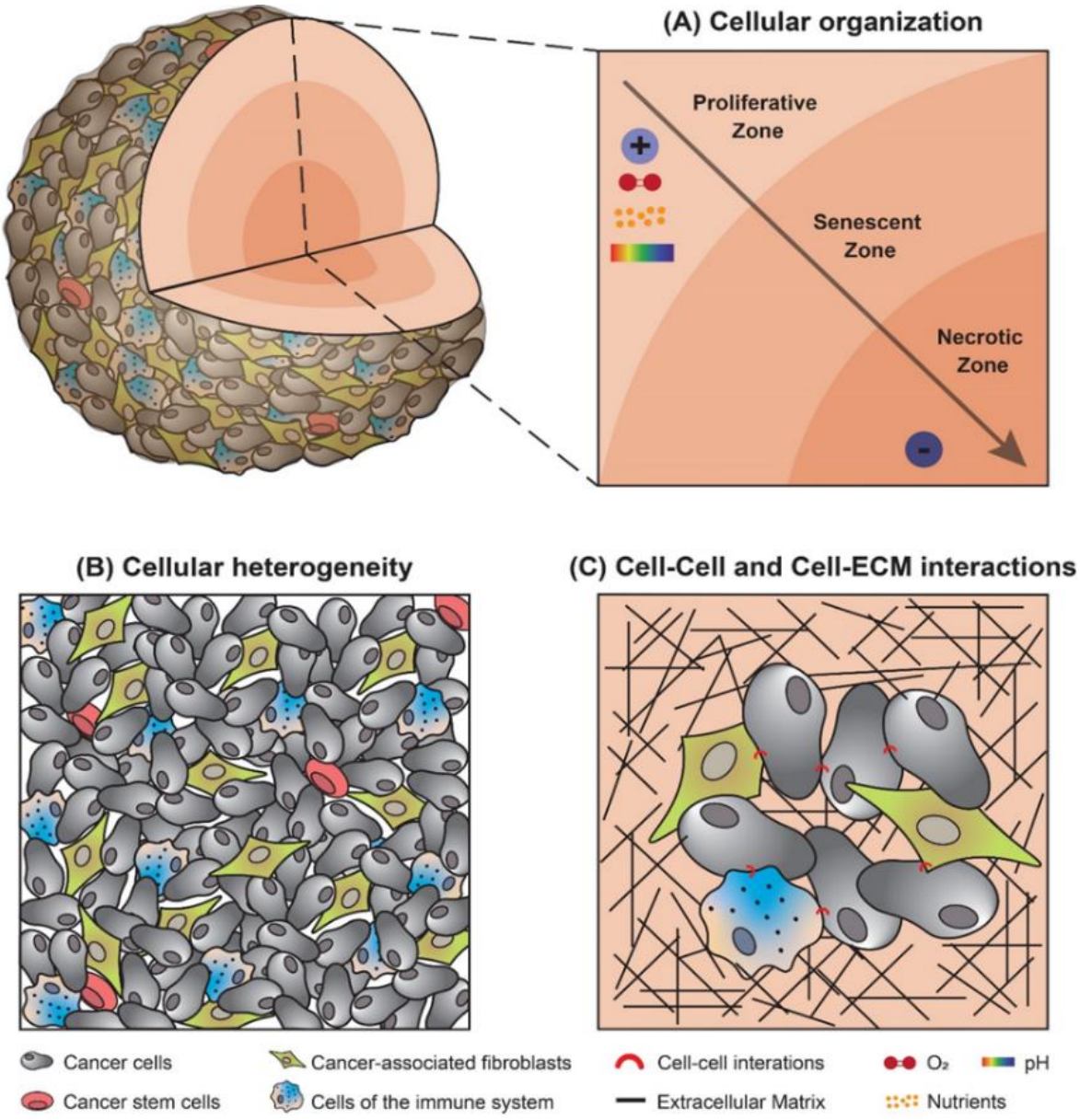

Figure 6: Schematic representation of spheroids' properties. Spheroids display a 3-layered organization with gradients of oxygen, nutrients and pH (A). Representation of the cellular heterogeneity (B), and cell-cell and cell-ECM interactions (C) occurring in the spheroids (Adapted from [92]).

Spheroids display a 3-layered organization, containing proliferative, quiescent and necrotic cells [93, 94]. Spheroids' outer layer is composed of highly proliferative cells with unrestricted access to oxygen and nutrients [94]. On the other hand, quiescent cells are found in the spheroids' middle layer, while necrotic cells are present in spheroids' inner layer (core), being deprived of oxygen and nutrients [93-95]. In this way, cells in spheroids' interior are weakly affected by pharmaceuticals that act by suppressing cells' proliferation (*e.g.* paclitaxel) [96, 97]. In turn, spheroids' hypoxic environment leads to: i) an upregulation of the expression of HIF-1α (which has been linked to an upregulation of

antiapoptotic proteins and P-gp; ii) resistance to therapeutics whose action relies on the production of reactive oxygen species (ROS) (*e.g*. DOX); iii) acidification of the spheroids' core (as a result of the conversion of pyruvate to lactate to obtain energy – Warburg effect) [98-100]. Furthermore, spheroids can also display a higher resistance to hyperthermia mediated death, a phenomenon that has been correlated with their higher Heat Shock Protein 70 (HSP70) expression [101-104].

The acidic environment found within spheroids affects the penetration and uptake of therapeutics [100, 105, 106]. This penetration barrier is also supported by the ECM components (*e.g*. collagen and elastin) secreted by the spheroids' cells, as well as by the cell-cell and cell-ECM physical interactions occurring in spheroids [107, 108]. These interactions are responsible for the establishment of a high interstitial fluid pressure that hinders therapeutics' penetration [107, 109]. As importantly, the cell-cell interactions established between the cancer cells, cancer stem cells and stromal cells occurring within spheroids can enable signaling pathways enrolled in therapeutics' resistance, namely the HIF-1 and NOTCH pathways [89, 110-112].

In this way, spheroids appear to be a promising 3D *in vitro* cancer model for the evaluation of chemo-PTT mediated by nanomaterials.

1.4. Aims

The aim of this Master thesis plan was to evaluate the effect of sulfobetaine methacrylate functionalized BSA nanoparticles (SBMA-BSA NPs) mediated' PTT, chemotherapy and chemo-PTT towards 2D and 3D *in vitro* cancer models.

The specific aims of this dissertation are:

- Formulation of SBMA-BSA NPs incorporating IR780 and the IR780-DOX combination;
- Characterization of the physicochemical and optical properties of both nanoformulations;
- Evaluation of the nanoparticles' mediated PTT, chemotherapy and chemo-PTT in monolayers of cancer cells (2D *in vitro* models);
- Evaluation of the nanoparticles' mediated PTT, chemotherapy and chemo-PTT in spheroids (3D *in vitro* models);

Chapter 2

Experimental Section

2. Experimental Section

2.1. Materials

Michigan Cancer Foundation-7 (MCF-7) and Normal Human Dermal Fibroblast (NHDF) cell lines were obtained from ATCC (Middlesex, UK) and Promocell (Heidelberg, Germany), respectively. Acetone and methanol were acquired from Fisher Scientific (Oeiras, Portugal). Fetal Bovine Serum (FBS) was purchased from Biochrom AG (Berlin, Germany). DOX was obtained from Carbosynth (Berkshire, UK). DL-Dithiothreitol (DTT), Dulbecco's Modified Eagle's Medium F12 (DMEM-F12), resazurin, [2-(Methacryloyloxy) ethyl] dimethyl-(3-sulfopropyl) ammonium hydroxide (SBMA), and IR780 iodide were supplied by Sigma-Aldrich (Sintra, Portugal). Agarose was obtained from Grisp (Porto, Portugal). BSA was purchased to Amresco (Pennsylvania, EUA). T-Flasks and cell culture plates were acquired from Thermo Fisher Scientific (Porto, Portugal). Double deionized water was used in all the required assays (0.22 μm filtered, 18.2 MΩ cm).

2.2. Methods

2.2.1. Synthesis and characterization of SBMA-*g*-BSA

The synthesis process of the BSA grafted with SBMA (SBMA-*g*-BSA) was performed as previously described by Alves and co-workers [37]. Briefly, 194 mg of SBMA and 250 mg of BSA where dissolved in water (a molar excess of SBMA was used for the primary amine and thiol groups of BSA). Then, NaOH (1 M) was used to adjust the pH to 12 and the solution was stirred at 37 ºC for 24 h. After this step, the solution was dialyzed against water for 2 days (14 kDa molecular weight cut-off membrane) and freeze-dried (ScanVac CoolSafe, LaboGene ApS, Lynge, Denmark), yielding SBMA-*g*-BSA. Then, Fourier Transform Infrared Spectroscopy (FTIR) analysis using a Nicolet iS10 spectrometer (Thermo Scientific Inc., MA, USA) was used to confirm the successful synthesis of SBMA-*g*-BSA.

2.2.2. Preparation of IR+DOX/SBMA-BSA NPs and IR/SBMA-BSA NPs

The SBMA-BSA NPs co-encapsulating IR780 and Doxorubicin (IR+DOX/SBMA-BSA NPs) were formulated using the nanoprecipitation method as previously reported by Alves *et al.* [37]. Briefly, 5 mL of a Phosphate Buffered Saline (PBS) solution containing SBMA-*g*-BSA (5 mg) and DTT (386 μg) was allowed to react for 20 min under stirring. Then, DOX (100 μg) and IR780 (100 μg) dissolved in acetone were added dropwise to the polymer-DTT solution during 2 h (room temperature, under stirring). Afterwards, the solution was recovered and dialyzed against water (500-1000 Da molecular weight cut-off membrane),

yielding IR+DOX/SBMA-BSA NPs. The same procedure was employed to formulate IR780 loaded SBMA-BSA NPs using 250 μg of IR780 (IR/SBMA-BSA NPs).

2.2.3. Characterization of the physicochemical, optical and photothermal properties of the IR/SBMA-BSA NPs and IR+DOX/SBMA-BSA NPs

IR/SBMA-BSA NPs and IR+DOX/SBMA-BSA NPs size distribution (in water) and zeta potential (in PBS (10 mM of Na_2HPO_4)) were evaluated on a Zetasizer Nano ZS (Malvern Instruments Ltd., Worcestershire, UK). The morphology of both nanoformulations was confirmed by Transmission Electron Microscopy (TEM). For this purpose, the nanoformulations were stained with phosphotungstic acid (2 % (w/v)) and then imaged on a Hitachi-HT7700 transmission electron microscope (Hitachi Ltd., Tokyo, Japan), operated at an accelerating voltage of 80-100 kV. The NIR absorption of the nanoformulations was determined in an Evolution 201 spectrophotometer (Thermo Scientific Inc.). For such, the absorption spectra of IR/SBMA-BSA NPs and IR+DOX/SBMA-BSA NPs in water (1.25 μg mL^{-1} of IR780 equivalents) and of free IR780 in methanol (1.25 μg mL^{-1}) were acquired. The photothermal capacity of IR+DOX/SBMA-BSA NPs (at different concentrations of IR780 equivalents) was determined by irradiating the samples with NIR light (808 nm, 1.7 W cm^{-2}) during 5 min, and recording the temperature changes using a thermocouple thermometer [113].

To determine the IR780 encapsulation efficiency, the samples' absorbance at 780 nm in a water:methanol (1:1 (v/v)) solution was analysed, as previously described by Alves *et al.* [37]. In turn, to analyze the encapsulation efficiency of DOX, the fluorescence emitted by the samples (λ_{ex} = 488 nm, λ_{em} = 590 nm) was analyzed in a Spectramax Gemini EM spectrofluorometer (Molecular Devices LLC, California, USA) [40].

2.2.4. Evaluation of the therapeutic effect of IR/SBMA-BSA NPs and IR+DOX/SBMA-BSA NPs towards 2D cancer models

The therapeutic effect mediated by IR/SBMA-BSA NPs and IR+DOX/SBMA-BSA NPs towards MCF-7 cells was determined using the resazurin assay, as previously described [40]. For such, cells were cultured in DMEM-F12 medium supplemented with 10 % (v/v) of FBS and 1 % (v/v) of streptomycin/gentamycin in a humidified incubator (37 °C, 5 % CO_2). MCF-7 cells were seeded in 96-well plates at a density of 1×10^4 cells per well. After 24 h, cells were incubated with fresh culture medium containing different concentrations of IR/SBMA-BSA NPs (IR780: 1.00 or 3.00 μg mL^{-1}) or IR+DOX/SBMA-BSA NPs (IR780/DOX: 1.00/0.66 μg mL^{-1} or 3.00/1.98 μg mL^{-1}). After 4 h, the cells were irradiated

with NIR light for 5 min (808 nm, 1.7 W cm^{-2}). After 24 h of incubation, the culture medium was replaced with fresh medium containing resazurin (10 % (v/v)) and the cells were incubated for 4 h in the dark (37 °C, 5 % CO_2). Subsequently, the cells' viability was determined by measuring the fluorescence of resorufin (λ_{ex} = 560 nm; λ_{em} = 590 nm, Spectramax Gemini EM spectrofluorometer (Molecular Devices LLC, California, USA)). Cells incubated with ethanol (70 % (v/v)) and cells incubated solely with culture medium were used as positive control (K^+) and negative control (K^-), respectively.

2.2.5. Evaluation of the therapeutic effect of IR/SBMA-BSA NPs and IR+DOX/SBMA-BSA NPs towards 3D cancer models

3D tumor spheroids were produced as previously described [40, 114]. Briefly, agarose structures (2 % (w/v)) with spherical microwells were formed by using a micro-mold (3D Petri Dish®, Microtissues Inc., Providence RI, USA). Afterward, MCF-7 cells and NHDF at 1:1 cell ratio were seeded in the agarose structures (1×10^6 cells per structure), leading to the formation of 81 spheroids per agarose structure. The spheroids were cultured during a period of 10 days in DMEM-F12 medium supplemented with 10 % (v/v) of FBS and 1 % (v/v) of streptomycin/gentamycin, inside an incubator with a humidified atmosphere (37 °C, 5 % CO_2). The culture medium was changed every 2 days.

After the generation of the 3D spheroids, the therapeutic effect mediated by IR/SBMA-BSA NPs and IR+DOX/SBMA-BSA NPs was determined using the resazurin method as described above. Briefly, spheroids were incubated with DMEM-F12 containing IR/SBMA-BSA NPs (IR780: 3.00 μg mL^{-1} or 9.00 μg mL^{-1}) or IR+DOX/SBMA-BSA NPs (IR780/DOX: 3.00/1.98 μg mL^{-1} or 9.00/5.93 μg mL^{-1}) for 24 h. Each experimental condition was evaluated using 30 spheroids. Then, the spheroids were irradiated with NIR light (808 nm, 1.7 W cm^{-2}) for 5 min. After 48 h, the culture medium was replaced with fresh culture medium containing resazurin (10 % (v/v)). Finally, the viability of the cells within spheroids was determined as described in section 2.2.4.

2.2.6. Statistical Analysis

All data are presented as the mean ± standard deviation (S.D.). To analyze the data and compare different groups, the one-way analysis of variance (ANOVA) with the Student-Newman-Keuls test was used (GraphPad Prism 6 software). A value of p lower than 0.05 ($^*p < 0.05$) was considered statistically significant.

Chapter 3

Results and Discussion

3. Results and Discussion

3.1. Preparation and characterization of IR/SBMA-BSA NPs and IR+DOX/SBMA-BSA NPs

In order to compare the efficacy of the nanomaterials' mediated chemotherapy, PTT and chemo-PTT towards 2D and 3D *in vitro* cancer models, IR/SBMA-BSA NPs and IR+DOX/SBMA-BSA NPs were prepared (Figure 7). In a previous study performed by Alves and co-workers, an extensive characterization of the IR/SBMA-BSA NPs in 2D *in vitro* cancer models was done, and the data obtained demonstrated the cytocompatibility of the nanoparticles and that the SBMA functionalization improves the nanoformulations' colloidal stability and cellular uptake [37].

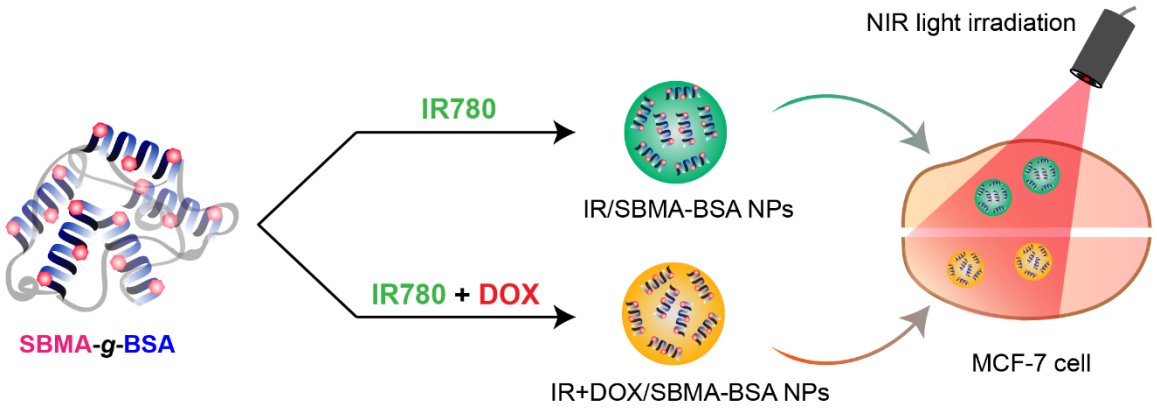

Figure 7: Schematic representation of the nanoparticles' assembly and application in cancer therapy.

Initially, the SBMA-*g*-BSA was synthesized following the protocol described by Alves and co-workers [37]. The FTIR spectrum of SBMA showed peaks at 1035 cm^{-1} and 1299 cm^{-1}, which correspond to the S=O stretch, and also presents a characteristic peak at 1715 cm^{-1}, corresponding to the C=O stretch (Figure 8 A). On the other hand, the FTIR spectrum of BSA had peaks corresponding to the O-H (3283 cm^{-1}), C-H (2872 cm^{-1} and 2958 cm^{-1}) and C=O (1644 cm^{-1}) vibrations (Figure 8 A). In turn, the spectrum of SBMA-*g*-BSA presented several peaks of the BSA functional groups, as well as the S=O stretch from SBMA, confirming the successful grafting of SBMA into BSA (Figure 8 A and B).

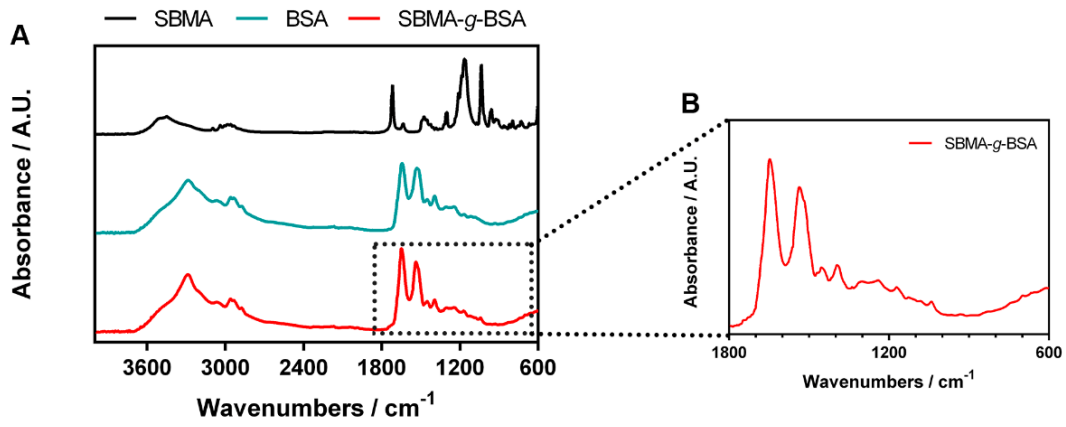

Figure 8: FTIR spectra of SBMA, BSA and SBMA-*g*-BSA (A). FTIR spectrum of SBMA-*g*-BSA in the 1800–600 cm^{-1} wavenumber range (B).

Then, the IR/SBMA-BSA NPs and IR+DOX/SBMA-BSA NPs were produced by the nanoprecipitation method due to its reliability and simplicity [37, 113]. The Dynamic Light Scattering (DLS) analysis revealed that IR/SBMA-BSA NPs have an average size of 97.2 ± 0.8 nm, while the IR+DOX/SBMA-BSA NPs display an average size of 92.3 ± 1.2 nm (n = 3; batch triplicates; Figure 9). The slightly lower size of the IR+DOX/SBMA-BSA NPs may be correlated to the different hydrophobic interactions occurring in the core of this nanoformulation. As importantly, the size of both nanoformulations is within the ideal range for tumor accumulation through the EPR effect [32, 115, 116]. The Polydispersity Index (PDI) of IR/SBMA-BSA NPs (0.196 ± 0.007) and IR+DOX/SBMA-BSA NPs (0.330 ± 0.019) is in agreement with that reported in other studies using nanoformulations loaded with IR780 and/or DOX [37, 40, 62, 113]. The zeta potential of the two nanoformulations was also measured. The results revealed that IR/SBMA-BSA NPs (-9.57 ± 0.81 mV) and IR+DOX/SBMA-BSA NPs (-9.55 ± 0.67 mV) have a similar surface charge. These charge values are in agreement to those reported in other studies using zwitterionic-based nanostructures and are also within the ideal range (-10 mV to 10 mV) for application in cancer therapy [34, 37, 117, 118].

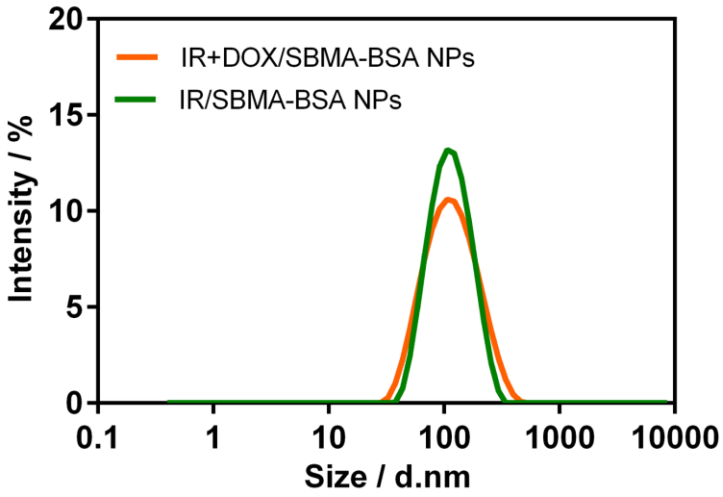

Figure 9: DLS size distribution of IR/SBMA-BSA NPs and IR+DOX/SBMA-BSA NPs.

The IR/SBMA-BSA NPs displayed a 53 % efficiency in encapsulating IR780. Interestingly, the IR+DOX/SBMA-BSA NPs had an IR780 and DOX encapsulation efficiency of 68 % and 45 %, respectively (Figure 10). Such may be correlated to stronger hydrophobic interactions occurring in the core of IR+DOX/SBMA-BSA NPs, leading to a higher drug entrapment. Similar findings have been previously reported for other nanoformulations co-encapsulating multiple agents [40, 119, 120].

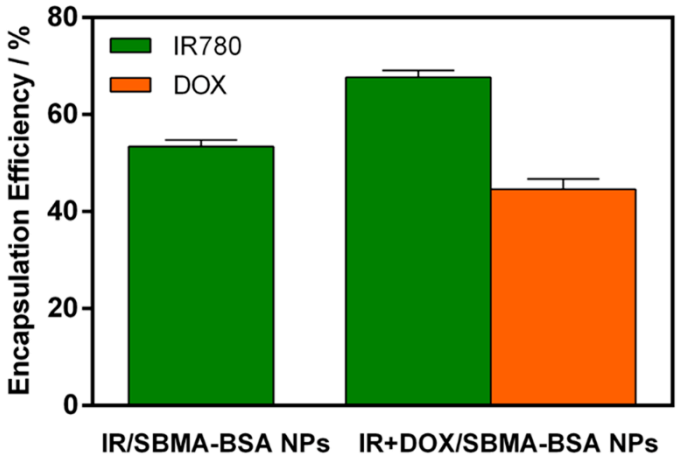

Figure 10: Encapsulation efficiency of IR780 and DOX in IR/SBMA-BSA NPs and IR+DOX/SBMA-BSA NPs. Each bar represents mean ± S.D. (n = 3; batch triplicates).

Finally, the morphology of IR/SBMA-BSA NPs (Figure 11 A) and IR+DOX/SBMA-BSA NPs (Figure 11 B) was analyzed by TEM, revealing that both formulations have a spherical shape. This spherical morphology has also been observed in other formulations prepared by the nanoprecipitation technique [37, 40, 119]. Furthermore, this shape has also been associated with a better internalization by cancer cells and higher tumor uptake [34, 113, 121].

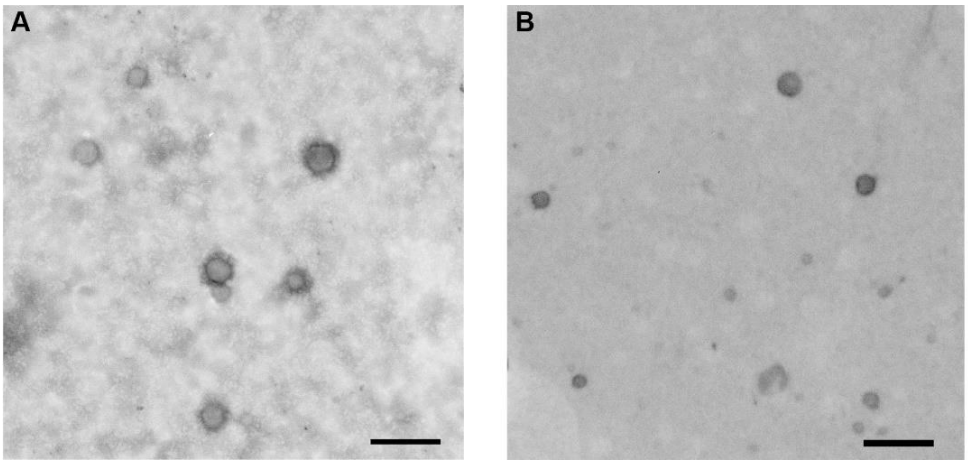

Figure 11: TEM analysis of IR/SBMA-BSA NPs (A) and IR+DOX/SBMA-BSA NPs (B). Scale bars correspond to 200 nm.

3.2. NIR absorption and photothermal capacity of IR/SBMA-BSA NPs and IR+DOX/SBMA-BSA NPs

In order to characterize the capacity of the nanoformulations to interact with the NIR light, their absorption spectra were acquired (Figure 12 A). As expected, free IR780 (dissolved in methanol) demonstrated a higher absorption in the NIR region, with a maximum absorption peak at 780 nm (Figure 12 A). When the IR780 was encapsulated in IR/SBMA-BSA NPs and in IR+DOX/SBMA-BSA NPs, its absorption spectrum suffered a red-shift (Figure 12 A). Due to this shift into the NIR range, the absorption of IR/SBMA-BSA NPs and IR+DOX/SBMA-BSA NPs at 808 nm was 1.03-fold and 1.35-fold greater than that of free IR780, respectively. This deviation of the IR/SBMA-BSA NPs and IR+DOX/SBMA-BSA NPs absorptions towards the NIR zone has been attributed to changes in solvents' polarity and/or to different hydrophobic interactions occurring in the nanoparticles' core [37, 40, 42, 119]. Considering that 808 nm light was used in the photothermal experiments, the higher absorption of the nanoformulations at this wavelength may lead to a greater therapeutic outcome.

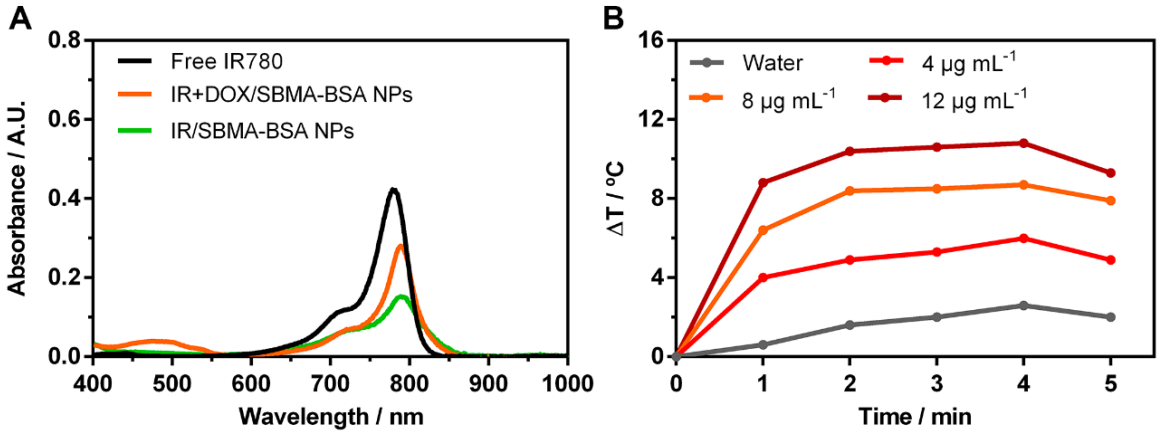

Figure 12: Characterization of the optical properties and photothermal capacity of SBMA-BSA NPs. Absorption spectra of free IR780 (1.25 μg mL^{-1}; in methanol), and of IR/SBMA-BSA NPs and IR+DOX/SBMA-BSA NPs (1.25 μg mL^{-1} of IR780 equivalents; in water) (A). Photoinduced heat produced by IR+DOX/SBMA-BSA NPs during 5 min of irradiation (808 nm, 1.7 W cm^{-2}) (B).

Subsequently, the photothermal capacity of IR+DOX/SBMA-BSA NPs was evaluated (Figure 12 B). For such, the IR+DOX/SBMA-BSA NPs (containing different concentrations of IR780) were irradiated with NIR light (808 nm, 1.7 W cm^{-2}) for 5 min and the temperature changes were recorded (Figure 12 B). At the maximum concentration tested (12.00 μg mL^{-1} of IR780 equivalents), the IR+DOX/SBMA-BSA NPs could generate a temperature increase of 11.0 °C, which is sufficiently high to induce damage to cancer cells [32]. The photothermal capacity of IR/SBMA-BSA NPs was described in a previous publication by Alves and co-workers [37]. At a concentration of 8.00 μg mL^{-1} of IR780 equivalents, the IR/SBMA-BSA NPs were able to produce a maximum temperature increase of about 7 °C (808 nm, 1.7 W cm^{-2}) [37]. Herein, at the same concentration and laser intensity, the IR+DOX/SBMA-BSA NPs produced a maximum temperature increase of 9.0 °C (Figure 12 B). The slightly higher photothermal capacity of IR+DOX/SBMA-BSA NPs may be related to their greater absorption at 808 nm (Figure 12 A). As importantly, water exposed to NIR light (control) did not suffer a meaningful temperature increase. Such is in agreement with the weak interaction of 808 nm radiation with water [40] and demonstrates that IR+DOX/SBMA-BSA NPs can produce an on-demand therapeutic effect.

Lu *et al.* showed that IR780 loaded PEGylated zwitterionic nanoparticles could produce a temperature increase of about 11 °C using an IR780 concentration of 27 μg mL^{-1} and laser intensity of 1.0 W cm^{-2} [122]. The IR+DOX/SBMA-BSA NPs produced herein, generated a similar temperature increase (11.0 °C) using only 12.00 μg mL^{-1} and laser intensity of 1.7 W cm^{-2}, confirming their good photothermal potential.

3.3. Therapeutic effect mediated by IR/SBMA-BSA NPs and IR+DOX/SBMA-BSA NPs in 2D cancer models

The effect of nanomaterials' mediated PTT (IR/SBMA-BSA NPs and NIR light), chemotherapy (IR+DOX/SBMA-BSA NPs), and chemo-PTT (IR+DOX/SBMA-BSA NPs and NIR light) towards monolayers of MCF-7 cells (2D *in vitro* model) was then investigated (Figure 13 A).

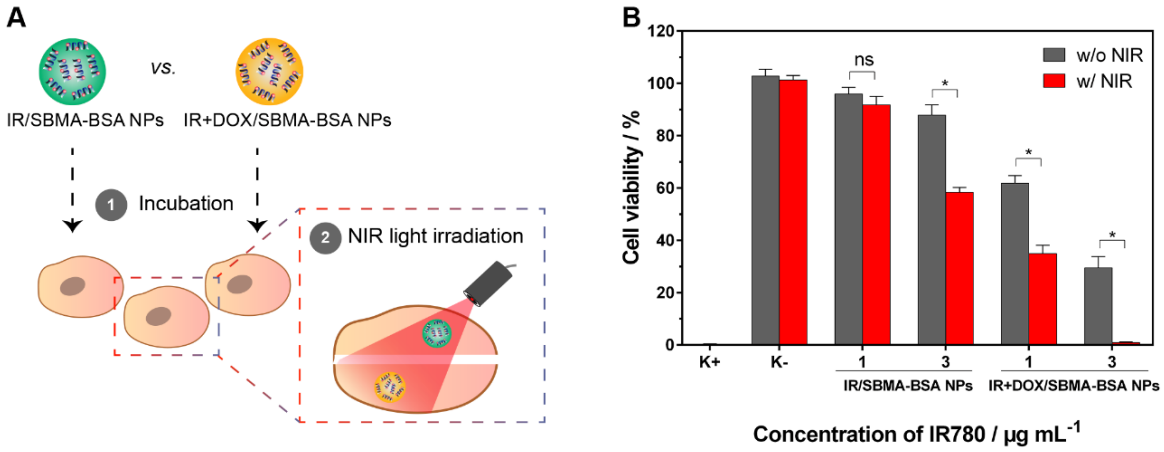

Figure 13: Determination of the therapeutic capacity of IR/SBMA-BSA NPs and IR+DOX/SBMA-BSA NPs using 2D *in vitro* cancer models (monolayers of cancer cells). Schematic representation of the procedure used to evaluate the nanoparticles' singles and combinatorial therapies towards MCF-7 cells (A). Therapeutic effect mediated by SBMA-BSA NPs towards MCF-7 cells without (w/o NIR) and with NIR (w/ NIR) laser irradiation (808 nm, 1.7 W cm^{-2}, 5 min) (B). K^+ represents the positive control. K^- w/o NIR represents the negative control, while K^- w/ NIR represents cells solely treated with NIR light. Data represent mean ± S.D., n = 5, (*$p < 0.0001$), ns = non-significant.

As expected, MCF-7 cells treated with only IR/SBMA-BSA NPs (without NIR light; 3.00 μg mL^{-1} of IR780 equivalents) demonstrated a high viability (> 87 %) (Figure 13 B). This result is in agreement with the fact that IR780 loaded nanoformulations are generally non-cytotoxic when not irradiated with NIR light [40, 71]. Moreover, cells solely exposed to NIR light did not suffer alterations on their viability, which is explained by the minimal/insignificant interactions of this radiation with biological components (Figure 13 B).

In turn, at the same IR780 dose (3.00 μg mL^{-1} of IR780 equivalents), cells treated with IR/SBMA-BSA NPs and NIR light (nanomaterials' mediated PTT) had their viability diminished to about 58 % (Figure 13 B). Such indicates that the photothermal heating mediated by IR/SBMA-BSA NPs is capable of generating a therapeutic effect.

On the other hand, when these cells were incubated with IR+DOX/SBMA-BSA NPs (3.00 μg mL^{-1} of IR780; 1.98 μg mL^{-1} of DOX) without laser irradiation (nanomaterials' mediated chemotherapy), there was a reduction of their viability to about 29 % (Figure 13 B). By combining IR+DOX/SBMA-BSA NPs with NIR radiation (nanomaterials mediated' chemo-PTT), the cells' viability was further reduced to about 1 % (Figure 13 B). By screening these 3 different therapeutic modalities in 2D *in vitro* cancer models, it was possible to conclude that both the nanomaterials' mediated PTT and chemotherapy can promote a therapeutic effect, being outperformed by the nanomaterials' mediated chemo-PTT.

Alves *et al.* verified that the chemo-PTT mediated by DOX and IR780 loaded Hyaluronic acid-based micelles could reduce MCF-7 cells' viability to about 20 % (IR780/DOX: 3.5/1.9 μg mL^{-1}; 808 nm, 1.7 W cm^{-2}, 5 min) [40]. In another work, monolayers of cancer cells treated with IR780 and DOX loaded PEGylated micelles plus NIR radiation (IR780/DOX: 5.0/10.0 μg mL^{-1}, 808 nm, 4.0 W cm^{-2}, 5 min) suffered a decrease in their viability to about 22 % [65]. Compared to these studies, the IR+DOX/SBMA-BSA NPs in combination with NIR light could diminish cells' viability to 1 %, at a lower dose of therapeutics (IR780/DOX dose: 3.00/1.98 μg mL^{-1}) and using a similar or weaker intensity (808 nm, 1.7 W cm^{-2}, 5 min), hence demonstrating their potential for cancer chemo-PTT.

3.4. Therapeutic effect mediated by IR/SBMA-BSA NPs and IR+DOX/SBMA-BSA NPs in 3D cancer models

After evaluating the nanomaterials' mediated PTT, chemotherapy, and chemo-PTT in monolayers of cancer cells (2D *in vitro* model), the efficacy of these modalities towards spheroids (3D *in vitro* model) was also analysed (Figure 14 A).

In general, the different therapeutic modalities mediated by the nanomaterials had a weaker effect on spheroids (Figure 14 B) when compared to their outcome in the conventional 2D cultures (Figure 13 B). This behavior has also been described in the literature for other nanostructures [40, 123, 124]. The nanoformulations' weaker effect on the spheroids can be justified by the ability of this 3D *in vitro* model to mimic key features of the *in vivo* solid tumors, including penetration and resistance patterns [78, 125].

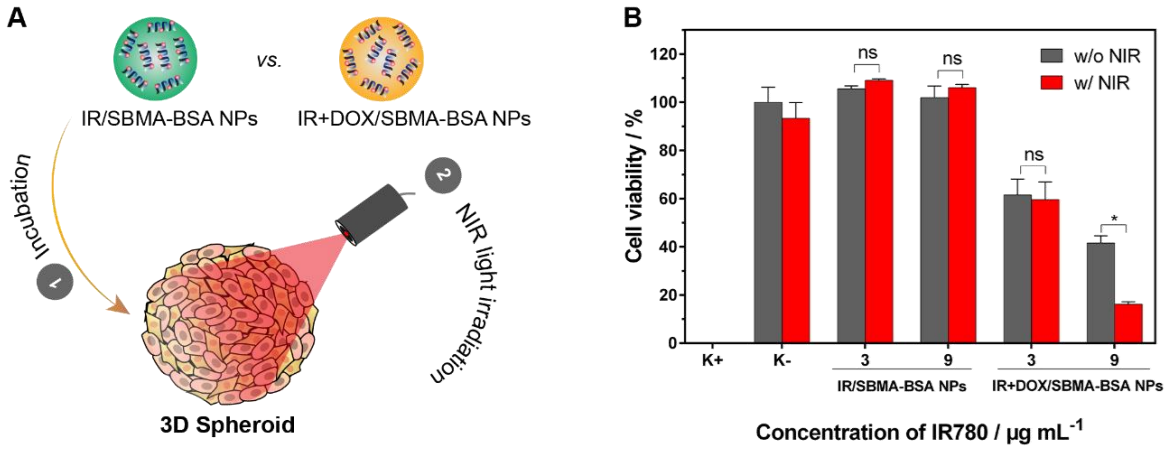

Figure 14: Determination of the therapeutic capacity of IR/SBMA-BSA NPs and IR+DOX/SBMA-BSA NPs using 3D *in vitro* cancer models (tumor spheroids). Schematic representation of the procedure used to evaluate the nanoparticles' singles and combinatorial therapies towards spheroids (A). Therapeutic effect mediated by SBMA-BSA NPs towards spheroids without (w/o NIR) and with NIR (w/ NIR) laser irradiation (808 nm, 1.7 W cm^{-2}, 5 min) (B). K^+ represents the positive control. K^- w/o NIR represents the negative control, while K^- w/ NIR represents spheroids solely treated with NIR light. Data represent mean ± S.D., n = 30, (*$p < 0.0001$), ns = non-significant.

Interestingly, spheroids treated with IR/SBMA-BSA NPs plus NIR light (nanomaterials' mediated PTT) did not have their viability affected even at a high IR780 dose (9.00 µg mL^{-1}) – Figure 14 B. Such may be related to the fact that spheroids display a higher resistance to temperature-mediated cell death [104]. Considering that nanomaterials' mediated PTT was effective on the cancer cell monolayers, this result highlights the value of using spheroids to attain a more realistic determination of the therapeutic capacity of the nanomaterials *in vitro*.

In turn, spheroids treated with only IR+DOX/SBMA-BSA NPs (nanomaterials' mediated chemotherapy) suffered a reduction on their viability to about 42 % (Figure 14 B). By further combining IR+DOX/SBMA-BSA NPs with NIR light (nanomaterials' mediated chemo-PTT), a synergistic decrease of spheroids viability to about 16 % was achieved (Figure 14 B), indicating that this is the most effective therapeutic modality.

Chen *et al.* produced PEGylated CuS based micelles loaded with aminoflavone, whose chemo-PTT was able to reduce spheroids' viability to about 46 % (980 nm, 0.75 W cm^{-2}, 10 min, 0.05 µg mL^{-1} of aminoflavone) [124]. In another study, Su *et al.* verified that the chemo-PTT induced by transferrin functionalized PEGylated reduced graphene oxide-based hybrids loaded with DTX and perfluorohexane could reduce spheroids cells' viability to about 2 % (808 nm, 2.0 W cm^{-2}, 10 min, 20 µg mL^{-1} of graphene derivatives) [126]. Herein, the chemo-PTT mediated by IR+DOX/SBMA-BSA NPs could reduce spheroids viability to 16 %, with only 9.00/5.93 µg mL^{-1} of IR780/DOX and with only 5 min of

irradiation (808 nm, 1.7 W cm^{-2}). Together, these results demonstrate that IR+DOX/SBMA-BSA NPs are promising agents for breast cancer chemo-PTT.

Chapter 4

Conclusion and Future Perspectives

4. Conclusion and Future Perspectives

Despite the scientific advances in the field of breast cancer treatment, this disease still prevails as one of the deadliest worldwide. This scenario can be attributed to the lack of effectiveness of the conventional therapies (*e.g.* chemotherapy and radiotherapy), as well as to their systemic toxicity (which is responsible for numerous side effects in patients).

Recently, researches have focused their efforts in the development of nanomaterials aimed for chemo-PTT due to their capacity to produce a spatio-temporal controlled anti-cancer effect. During the development of these nanomaterials, their therapeutic capacity is initially assessed using monolayers of cancer cells (2D *in vitro* model). Based on the data gathered with the 2D *in vitro* models, the best nanoformulations are selected for further evaluation in tumor bearing mice (*in vivo* model). However, the 2D *in vitro* models are not capable of mimicking all the key features of the *in vivo* solid tumors, contributing for the selection of nanomedicines that later fail to demonstrate efficacy *in vivo*. To overcome this critical limitation, the use of spheroids (3D *in vitro* models) has recently emerged in the pre-clinical drug discovery stage. In fact, spheroids are able to mimic the main properties of the *in vivo* solid tumors, namely: i) their 3D architecture, ii) microenvironment (gradients of nutrients, pH and gases), iii) cellular and acellular composition, and iv) biochemical and physical resistance patterns to the therapeutics.

In this Master thesis, the effect of the SBMA-BSA nanoparticles mediated' PTT (IR/SBMA-BSA NPs and NIR irradiation), chemotherapy (IR+DOX/SBMA-BSA NPs) and chemo-PTT (IR+DOX/SBMA-BSA NPs and NIR irradiation) was investigated in monolayers of cancer cells (2D *in vitro* model) and spheroids (3D *in vitro* model). In monolayers of cancer cells, the PTT mediated by nanoparticles was able to reduce cells' viability to about 58 %, while the chemotherapy mediated by nanomaterials led to a decrease in the cells' viability to 29 %. The best therapeutic effect was accomplished with the combinatorial chemo-PTT mediated by nanoparticles, which induced a reduction in cells' viability to 1 %. Interestingly, the studies in spheroids demonstrated that the PTT mediated by the nanoparticles does not induce any cytotoxicity towards this 3D model. On the other hand, the chemotherapy mediated by the nanoparticles reduced the spheroids' viability to 42 %. In turn, the combinatorial chemo-PTT mediated by the nanostructures decreased the viability of the spheroids to 16 %, revealing that this is the most promising therapeutic modality.

Overall, the results obtained in this dissertation highlight the importance of using 3D spheroids during the *in vitro* screening of single and combinatorial therapies mediated by

nanomaterials. Furthermore, the emergence of spheroids in the drug discovery phase can also contribute to reduce the number of animals in research, as well as to accelerate the overall drug development process.

In the future, the evaluation of the *in vivo* therapeutic performance of these nanoformulations will be crucial to establish a correlation with the data obtained using the spheroids. Furthermore, it would also be interesting to test these formulations in spheroids cultured in microfluidic chips due to their capacity to mimic the *in vivo* dynamic flow conditions.

Chapter 5

Bibliographic References

5. Bibliographic References

[1] R.L. Siegel, K.D. Miller, A. Jemal, Cancer statistics, 2020, CA: A Cancer Journal for Clinicians, 70 (2020) 7-30.

[2] www.sns.gov.pt/noticias/2018/05/22/programa-para-a-terapia-do-cancro/ (acessed in 02/03/2020).

[3] A.K. Basu, DNA Damage, Mutagenesis and Cancer, International Journal of Molecular Sciences, 19 (2018) 970.

[4] Y. Liu, T. Yin, Y. Feng, M.M. Cona, G. Huang, J. Liu, S. Song, Y. Jiang, Q. Xia, J.V. Swinnen, Mammalian models of chemically induced primary malignancies exploitable for imaging-based preclinical theragnostic research, Quantitative Imaging in Medicine and Surgery, 5 (2015) 708-729.

[5] D. Hanahan, R.A. Weinberg, Hallmarks of Cancer: The Next Generation, Cell, 144 (2011) 646-674.

[6] D. Hanahan, R.A. Weinberg, Biological Hallmarks of Cancer, Holland-Frei Cancer Medicine, (2016).

[7] M. Castells, B. Thibault, J.-P. Delord, B. Couderc, Implication of Tumor Microenvironment in Chemoresistance: Tumor-Associated Stromal Cells Protect Tumor Cells from Cell Death, International Journal of Molecular Sciences, 13 (2012) 9545-9571.

[8] H. Ungefroren, S. Sebens, D. Seidl, H. Lehnert, R. Hass, Interaction of tumor cells with the microenvironment, Cell Communication and Signaling, 9 (2011) 18.

[9] E.C. de Bruin, J.P. Medema, Apoptosis and non-apoptotic deaths in cancer development and treatment response, Cancer Treatment Reviews, 34 (2008) 737-749.

[10] M.A. Jafri, S.A. Ansari, M.H. Alqahtani, J.W. Shay, Roles of telomeres and telomerase in cancer, and advances in telomerase-targeted therapies, Genome Medicine, 8 (2016) 69.

[11] H. Li, X. Fan, J. Houghton, Tumor microenvironment: the role of the tumor stroma in cancer, Journal of Cellular Biochemistry, 101 (2007) 805-815.

[12] W.G. Jiang, A.J. Sanders, M. Katoh, H. Ungefroren, F. Gieseler, M. Prince, S. Thompson, M. Zollo, D. Spano, P. Dhawan, Tissue invasion and metastasis: Molecular,

biological and clinical perspectives, in: Seminars in cancer biology, Elsevier, 2015, pp. S244-S275.

[13] www.ligacontracancro.pt/servicos/detalhe/url/programa-de-rastreio-de-cancro-da-mama/ (acessed in 08/03/2020).

[14] R. Shah, K. Rosso, S.D. Nathanson, Pathogenesis, prevention, diagnosis and treatment of breast cancer, World Journal of Clinical Oncology, 5 (2014) 283-298.

[15] Y. Feng, M. Spezia, S. Huang, C. Yuan, Z. Zeng, L. Zhang, X. Ji, W. Liu, B. Huang, W. Luo, Breast cancer development and progression: Risk factors, cancer stem cells, signaling pathways, genomics, and molecular pathogenesis, Genes & Diseases, 5 (2018) 77-106.

[16] Y.-S. Sun, Z. Zhao, Z.-N. Yang, F. Xu, H.-J. Lu, Z.-Y. Zhu, W. Shi, J. Jiang, P.-P. Yao, H.-P. Zhu, Risk Factors and Preventions of Breast Cancer, International Journal of Biological Sciences, 13 (2017) 1387-1397.

[17] B. Weigelt, M.J. Bissell, Unraveling the microenvironmental influences on the normal mammary gland and breast cancer, in: Seminars in cancer biology, Elsevier, 2008, pp. 311-321.

[18] K. Polyak, Breast cancer: origins and evolution, The Journal of Clinical Investigation, 117 (2007) 3155-3163.

[19] A.E. Place, S.J. Huh, K. Polyak, The microenvironment in breast cancer progression: biology and implications for treatment, Breast Cancer Research, 13 (2011) 227.

[20] S.D. Soysal, A. Tzankov, S.E. Muenst, Role of the Tumor Microenvironment in Breast Cancer, Pathobiology, 82 (2015) 142-152.

[21] X. Li, J. Kim, J. Yoon, X. Chen, Cancer-Associated, Stimuli-Driven, Turn on Theranostics for Multimodality Imaging and Therapy, Advanced Materials, 29 (2017) 1606857.

[22] X. Xue, A. Lindstrom, H. Qu, Y. Li, Recent advances on small-molecule nanomedicines for cancer treatment, Wiley Interdisciplinary Reviews: Nanomedicine and Nanobiotechnology, 12 (2020) e1607.

[23] F. Danhier, To exploit the tumor microenvironment: Since the EPR effect fails in the clinic, what is the future of nanomedicine?, Journal of Controlled Release, 244 (2016) 108-121.

[24] J. Cao, Z. Chen, J. Chi, Y. Sun, Y. Sun, Recent progress in synergistic chemotherapy and phototherapy by targeted drug delivery systems for cancer treatment, Artificial Cells, Nanomedicine, and Biotechnology, 46 (2018) 817-830.

[25] C.-Y. Zhao, R. Cheng, Z. Yang, Z.-M. Tian, Nanotechnology for Cancer Therapy Based on Chemotherapy, Molecules, 23 (2018) 826.

[26] C.R. Arnold, J. Mangesius, I.-I. Skvortsova, U. Ganswindt, The Role of Cancer Stem Cells in Radiation Resistance, Frontiers in Oncology, 10 (2020) 164.

[27] G. Tian, X. Zhang, Z. Gu, Y. Zhao, Recent Advances in Upconversion Nanoparticles-Based Multifunctional Nanocomposites for Combined Cancer Therapy, Advanced Materials, 27 (2015) 7692-7712.

[28] S. Shen, M. Liu, T. Li, S. Lin, R. Mo, Recent progress in nanomedicine-based combination cancer therapy using a site-specific co-delivery strategy, Biomaterials Science, 5 (2017) 1367-1381.

[29] W. Dai, X. Wang, G. Song, T. Liu, B. He, H. Zhang, X. Wang, Q. Zhang, Combination antitumor therapy with targeted dual-nanomedicines, Advanced Drug Delivery Reviews, 115 (2017) 23-45.

[30] R. Jadia, C. Scandore, P. Rai, Nanoparticles for Effective Combination Therapy of Cancer, International Journal of Nanotechnology and Nanomedicine, 1 (2016).

[31] C.G. Alves, R. Lima-Sousa, D. de Melo-Diogo, R.O. Louro, I.J. Correia, IR780 based nanomaterials for cancer imaging and photothermal, photodynamic and combinatorial therapies, International Journal of Pharmaceutics, 542 (2018) 164-175.

[32] D. de Melo-Diogo, C. Pais-Silva, D.R. Dias, A.F. Moreira, I.J. Correia, Strategies to Improve Cancer Photothermal Therapy Mediated by Nanomaterials, Advanced Healthcare Materials, 6 (2017) 1700073.

[33] I.A. Khawar, J.H. Kim, H.-J. Kuh, Improving drug delivery to solid tumors: Priming the tumor microenvironment, Journal of Controlled Release, 201 (2015) 78-89.

[34] C.F. Rodrigues, C.G. Alves, R. Lima-Sousa, A.F. Moreira, D. de Melo-Diogo, I.J. Correia, Inorganic-based drug delivery systems for cancer therapy, in: Advances and Avenues in the Development of Novel Carriers for Bioactives and Biological Agents, Elsevier, 2020, pp. 283-316.

[35] Y. Zhang, C. Yang, W. Wang, J. Liu, Q. Liu, F. Huang, L. Chu, H. Gao, C. Li, D. Kong, Co-delivery of doxorubicin and curcumin by pH-sensitive prodrug nanoparticle for combination therapy of cancer, Scientific Reports, 6 (2016) 21225.

[36] D. de Melo-Diogo, E.C. Costa, C.G. Alves, R. Lima-Sousa, P. Ferreira, R.O. Louro, I.J. Correia, POxylated graphene oxide nanomaterials for combination chemo-phototherapy of breast cancer cells, European Journal of Pharmaceutics and Biopharmaceutics, 131 (2018) 162-169.

[37] C.G. Alves, D. de Melo-Diogo, R. Lima-Sousa, I.J. Correia, IR780 loaded sulfobetaine methacrylate-functionalized albumin nanoparticles aimed for enhanced breast cancer phototherapy, International Journal of Pharmaceutics, 582 (2020) 119346.

[38] G. Liu, N. Gao, Y. Zhou, J. Nie, W. Cheng, M. Luo, L. Mei, X. Zeng, W. Deng, Polydopamine-Based "Four-in-One" Versatile nanoplatforms for targeted dual chemo and photothermal synergistic cancer therapy, Pharmaceutics, 11 (2019) 507.

[39] H. Meng, M. Liong, T. Xia, Z. Li, Z. Ji, J.I. Zink, A.E. Nel, Engineered Design of Mesoporous Silica Nanoparticles to Deliver Doxorubicin and P-glycoprotein siRNA to Overcome Drug Resistance in a Cancer Cell Line, ACS Nano, 4 (2010) 4539-4550.

[40] C.G. Alves, D. de Melo-Diogo, R. Lima-Sousa, E.C. Costa, I.J. Correia, Hyaluronic acid functionalized nanoparticles loaded with IR780 and DOX for cancer chemo-photothermal therapy, European Journal of Pharmaceutics and Biopharmaceutics, 137 (2019) 86-94.

[41] G. Tian, W. Yin, J. Jin, X. Zhang, G. Xing, S. Li, Z. Gu, Y. Zhao, Engineered design of theranostic upconversion nanoparticles for tri-modal upconversion luminescence/magnetic resonance/X-ray computed tomography imaging and targeted delivery of combined anticancer drugs, Journal of Materials Chemistry B, 2 (2014) 1379-1389.

[42] Y. Liu, P. Huang, X. Hou, F. Yan, Z. Jiang, J. Shi, X. Xie, J. Shen, Q. Fan, Z. Wang, Hybrid curcumin–phospholipid complex-near-infrared dye oral drug delivery system to

inhibit lung metastasis of breast cancer, International Journal of Nanomedicine, 14 (2019) 3311-3330.

[43] H. Meng, W.X. Mai, H. Zhang, M. Xue, T. Xia, S. Lin, X. Wang, Y. Zhao, Z. Ji, J.I. Zink, Codelivery of an Optimal Drug/siRNA Combination Using Mesoporous Silica Nanoparticles to Overcome Drug Resistance in Breast Cancer in Vitro and in Vivo, ACS Nano, 7 (2013) 994-1005.

[44] S.W. Morton, M.J. Lee, Z.J. Deng, E.C. Dreaden, E. Siouve, K.E. Shopsowitz, N.J. Shah, M.B. Yaffe, P.T. Hammond, A Nanoparticle-Based Combination Chemotherapy Delivery System for Enhanced Tumor Killing by Dynamic Rewiring of Signaling Pathways, Science Signaling, 7 (2014) ra44.

[45] Y. Chen, Y. Gao, H. Chen, D. Zeng, Y. Li, Y. Zheng, F. Li, X. Ji, X. Wang, F. Chen, Engineering Inorganic Nanoemulsions/Nanoliposomes by Fluoride-Silica Chemistry for Efficient Delivery/Co-Delivery of Hydrophobic Agents, Advanced Functional Materials, 22 (2012) 1586-1597.

[46] B. Xiao, L. Ma, D. Merlin, Nanoparticle-mediated co-delivery of chemotherapeutic agent and siRNA for combination cancer therapy, Expert Opinion on Drug Delivery, 14 (2017) 65-73.

[47] C. Murugan, V. Sharma, R.K. Murugan, G. Malaimegu, A. Sundaramurthy, Two-dimensional cancer theranostic nanomaterials: Synthesis, surface functionalization and applications in photothermal therapy, Journal of Controlled Release, 299 (2019) 1-20.

[48] J. Chen, C. Ning, Z. Zhou, P. Yu, Y. Zhu, G. Tan, C. Mao, Nanomaterials as photothermal therapeutic agents, Progress in Materials Science, 99 (2019) 1-26.

[49] R. Lima-Sousa, D. de Melo-Diogo, C.G. Alves, E.C. Costa, P. Ferreira, R.O. Louro, I.J. Correia, Hyaluronic acid functionalized green reduced graphene oxide for targeted cancer photothermal therapy, Carbohydrate Polymers, 200 (2018) 93-99.

[50] C.F. Rodrigues, C.A. Reis, A.F. Moreira, P. Ferreira, I.J. Correia, Optimization of gold core-mesoporous silica shell functionalization with TPGS and PEI for cancer therapy, Microporous and Mesoporous Materials, 285 (2019) 1-12.

[51] L. Yuwen, J. Zhou, Y. Zhang, Q. Zhang, J. Shan, Z. Luo, L. Weng, Z. Teng, L. Wang, Aqueous phase preparation of ultrasmall MoSe 2 nanodots for efficient photothermal therapy of cancer cells, Nanoscale, 8 (2016) 2720-2726.

[52] D. Hu, J. Zhang, G. Gao, Z. Sheng, H. Cui, L. Cai, Indocyanine Green-Loaded Polydopamine-Reduced Graphene Oxide Nanocomposites with Amplifying Photoacoustic and Photothermal Effects for Cancer Theranostics, Theranostics, 6 (2016) 1043-1052.

[53] S. Li, Z. Sun, G. Deng, X. Meng, W. Li, D. Ni, J. Zhang, P. Gong, L. Cai, Dual-modal imaging-guided highly efficient photothermal therapy using heptamethine cyanine-conjugated hyaluronic acid micelles, Biomaterials Science, 5 (2017) 1122-1129.

[54] B. Xia, B. Wang, Z. Chen, Q. Zhang, J. Shi, Near-Infrared Light-Triggered Intracellular Delivery of Anticancer Drugs Using Porous Silicon Nanoparticles Conjugated with IR820 Dyes, Advanced Materials Interfaces, 3 (2016) 1500715.

[55] G.-Y. Pan, H.-R. Jia, Y.-X. Zhu, F.-G. Wu, Turning double hydrophilic into amphiphilic: IR825-conjugated polymeric nanomicelles for near-infrared fluorescence imaging-guided photothermal cancer therapy, Nanoscale, 10 (2018) 2115-2127.

[56] N. Fernandes, C.F. Rodrigues, A.F. Moreira, I.J. Correia, Overview of the application of inorganic nanomaterials in cancer photothermal therapy, Biomaterials Science, 8 (2020) 2990-3020.

[57] A.M. Smith, M.C. Mancini, S. Nie, Bioimaging: second window for in vivo imaging, Nature Nanotechnology, 4 (2009) 710-711.

[58] D. de Melo-Diogo, R. Lima-Sousa, C.G. Alves, I.J. Correia, Graphene family nanomaterials for application in cancer combination photothermal therapy, Biomaterials Science, 7 (2019) 3534-3551.

[59] M. Khafaji, M. Zamani, M. Golizadeh, O. Bavi, Inorganic nanomaterials for chemo/photothermal therapy: a promising horizon on effective cancer treatment, Biophysical Reviews, 11 (2019) 335-352.

[60] D. de Melo-Diogo, C. Pais-Silva, E.C. Costa, R.O. Louro, I.J. Correia, D-α-tocopheryl polyethylene glycol 1000 succinate functionalized nanographene oxide for cancer therapy, Nanomedicine, 12 (2017) 443-456.

[61] Z. Yang, R. Cheng, C. Zhao, N. Sun, H. Luo, Y. Chen, Z. Liu, X. Li, J. Liu, Z. Tian, Thermo-and ph-dual responsive polymeric micelles with upper critical solution temperature behavior for photoacoustic imaging-guided synergistic chemo-photothermal therapy against subcutaneous and metastatic breast tumors, Theranostics, 8 (2018) 4097-4115.

[62] F. Yan, W. Duan, Y. Li, H. Wu, Y. Zhou, M. Pan, H. Liu, X. Liu, H. Zheng, NIR-Laser-Controlled Drug Release from DOX/IR-780-Loaded Temperature-Sensitive-Liposomes for Chemo-Photothermal Synergistic Tumor Therapy, Theranostics, 6 (2016) 2337-2351.

[63] W. Li, J. Peng, L. Tan, J. Wu, K. Shi, Y. Qu, X. Wei, Z. Qian, Mild photothermal therapy/photodynamic therapy/chemotherapy of breast cancer by Lyp-1 modified Docetaxel/IR820 Co-loaded micelles, Biomaterials, 106 (2016) 119-133.

[64] A. Yuan, W. Huan, X. Liu, Z. Zhang, Y. Zhang, J. Wu, Y. Hu, NIR Light-Activated Drug Release for Synergetic Chemo–Photothermal Therapy, Molecular Pharmaceutics, 14 (2017) 242-251.

[65] Y. Deng, F. Käfer, T. Chen, Q. Jin, J. Ji, S. Agarwal, Let There be Light: Polymeric Micelles with Upper Critical Solution Temperature as Light-Triggered Heat Nanogenerators for Combating Drug-Resistant Cancer, Small, 14 (2018) 1802420.

[66] Q. Yang, Y. Xiao, Y. Yin, G. Li, J. Peng, Erythrocyte Membrane-Camouflaged IR780 and DTX Coloading Polymeric Nanoparticles for Imaging-Guided Cancer Photo–Chemo Combination Therapy, Molecular Pharmaceutics, 16 (2019) 3208-3220.

[67] J. Chen, H. Liu, C. Zhao, G. Qin, G. Xi, T. Li, X. Wang, T. Chen, One-step reduction and PEGylation of graphene oxide for photothermally controlled drug delivery, Biomaterials, 35 (2014) 4986-4995.

[68] M. Zheng, C. Yue, Y. Ma, P. Gong, P. Zhao, C. Zheng, Z. Sheng, P. Zhang, Z. Wang, L. Cai, Single-Step Assembly of DOX/ICG Loaded Lipid–Polymer Nanoparticles for Highly Effective Chemo-Photothermal Combination Therapy, ACS Nano, 7 (2013) 2056-2067.

[69] Z. Li, H. Wang, Y. Chen, Y. Wang, H. Li, H. Han, T. Chen, Q. Jin, J. Ji, pH-and NIR Light-Responsive Polymeric Prodrug Micelles for Hyperthermia-Assisted Site-Specific Chemotherapy to Reverse Drug Resistance in Cancer Treatment, Small, 12 (2016) 2731-2740.

[70] M.M. Leitão, D. de Melo-Diogo, C.G. Alves, R. Lima-Sousa, I.J. Correia, Prototypic Heptamethine Cyanine Incorporating Nanomaterials for Cancer Phototheragnostic, Advanced Healthcare Materials, 9 (2020) 1901665.

[71] D. Wang, S. Zhang, T. Zhang, G. Wan, B. Chen, Q. Xiong, J. Zhang, W. Zhang, Y. Wang, Pullulan-coated phospholipid and Pluronic F68 complex nanoparticles for carrying IR780 and paclitaxel to treat hepatocellular carcinoma by combining photothermal therapy/photodynamic therapy and chemotherapy, International Journal of Nanomedicine, 12 (2017) 8649-8670.

[72] X. Qiu, L. Xu, Y. Zhang, A. Yuan, K. Wang, X. Zhao, J. Wu, H. Guo, Y. Hu, Photothermal Ablation of in Situ Renal Tumor by PEG-IR780-C13 Micelles and Near-Infrared Irradiation, Molecular Pharmaceutics, 13 (2016) 829-838.

[73] C. Jiang, H. Cheng, A. Yuan, X. Tang, J. Wu, Y. Hu, Hydrophobic IR780 encapsulated in biodegradable human serum albumin nanoparticles for photothermal and photodynamic therapy, Acta Biomaterialia, 14 (2015) 61-69.

[74] L. Wang, S. Chen, Y. Zhu, M. Zhang, S. Tang, J. Li, W. Pei, B. Huang, C. Niu, Triple-Modal Imaging-Guided Chemo-Photothermal Synergistic Therapy for Breast Cancer with Magnetically Targeted Phase-Shifted Nanoparticles, ACS Applied Materials & Interfaces, 10 (2018) 42102-42114.

[75] X. Yuan, Y. Yin, W. Zan, X. Sun, Q. Yang, Hybrid manganese dioxide-bovine serum albumin nanostructure incorporated with doxorubicin and IR780 for enhanced breast cancer chemo-photothermal therapy, Drug Delivery, 26 (2019) 1254-1264.

[76] C. Wang, B. Huang, G. Yang, Y. Ouyang, J. Tian, W. Zhang, NIR-Triggered Multifunctional and Degradable Nanoplatform Based on an ROS-Sensitive Block Copolymer for Imaging-Guided Chemo-Phototherapy, Biomacromolecules, 20 (2019) 4218-4229.

[77] S. Breslin, L. O'Driscoll, Three-dimensional cell culture: the missing link in drug discovery, Drug Discovery Today, 18 (2013) 240-249.

[78] E.C. Costa, A.F. Moreira, D. de Melo-Diogo, V.M. Gaspar, M.P. Carvalho, I.J. Correia, 3D tumor spheroids: an overview on the tools and techniques used for their analysis, Biotechnology Advances, 34 (2016) 1427-1441.

[79] M. Kapałczyńska, T. Kolenda, W. Przybyła, M. Zajączkowska, A. Teresiak, V. Filas, M. Ibbs, R. Bliźniak, Ł. Łuczewski, K. Lamperska, 2D and 3D cell cultures–a comparison of different types of cancer cell cultures, Archives of Medical Science: AMS, 14 (2018) 910-919.

[80] M. Zhang, T. Wang, L. Zhang, L. Li, C. Wang, Near-Infrared Light and pH-Responsive Polypyrrole@ Polyacrylic acid/Fluorescent Mesoporous Silica Nanoparticles for Imaging and Chemo-Photothermal Cancer Therapy, Chemistry–A European Journal, 21 (2015) 16162-16171.

[81] Q. Chen, C. Wang, L. Cheng, W. He, Z. Cheng, Z. Liu, Protein modified upconversion nanoparticles for imaging-guided combined photothermal and photodynamic therapy, Biomaterials, 35 (2014) 2915-2923.

[82] J.Q. Peng, S. Fumoto, T. Suga, H. Miyamoto, N. Kuroda, S. Kawakami, K. Nishida, Targeted co-delivery of protein and drug to a tumor in vivo by sophisticated RGD-modified lipid-calcium carbonate nanoparticles, Journal of Controlled Release, 302 (2019) 42-53.

[83] X. Mu, F. Zhang, C. Kong, H. Zhang, W. Zhang, R. Ge, Y. Liu, J. Jiang, EGFR-targeted delivery of DOX-loaded Fe3O4@ polydopamine multifunctional nanocomposites for MRI and antitumor chemo-photothermal therapy, International Journal of Nanomedicine, 12 (2017) 2899-2911.

[84] X. Li, M. Takashima, E. Yuba, A. Harada, K. Kono, PEGylated PAMAM dendrimer–doxorubicin conjugate-hybridized gold nanorod for combined photothermal-chemotherapy, Biomaterials, 35 (2014) 6576-6584.

[85] G. Lazzari, P. Couvreur, S. Mura, Multicellular tumor spheroids: a relevant 3D model for the in vitro preclinical investigation of polymer nanomedicines, Polymer Chemistry, 8 (2017) 4947-4969.

[86] M. Millard, I. Yakavets, V. Zorin, A. Kulmukhamedova, S. Marchal, L. Bezdetnaya, Drug delivery to solid tumors: the predictive value of the multicellular tumor spheroid model for nanomedicine screening, International Journal of Nanomedicine, 12 (2017) 7993-8007.

[87] B.-W. Huang, J.-Q. Gao, Application of 3D cultured multicellular spheroid tumor models in tumor-targeted drug delivery system research, Journal of Controlled Release, 270 (2018) 246-259.

[88] N. Chaicharoenaudomrung, P. Kunhorm, P. Noisa, Three-dimensional cell culture systems as an in vitro platform for cancer and stem cell modeling, World Journal of Stem Cells, 11 (2019) 1065-1083.

[89] A.S. Nunes, A.S. Barros, E.C. Costa, A.F. Moreira, I.J. Correia, 3D tumor spheroids as in vitro models to mimic in vivo human solid tumors resistance to therapeutic drugs, Biotechnology and Bioengineering, 116 (2019) 206-226.

[90] S.A. Langhans, Three-Dimensional in Vitro Cell Culture Models in Drug Discovery and Drug Repositioning, Frontiers in Pharmacology, 9 (2018) 6.

[91] G. Hamilton, B. Rath, Applicability of tumor spheroids for in vitro chemosensitivity assays, Expert Opinion on Drug Metabolism & Toxicology, 15 (2019) 15-23.

[92] I. Mó, I.J. Sabino, D. de Melo-Diogo, R. Lima-Sousa, C.G. Alves, I.J. Correia, The importance of spheroids in analyzing nanomedicines' efficacy, Nanomedicine, (2020).

[93] S. Däster, N. Amatruda, D. Calabrese, R. Ivanek, E. Turrini, R.A. Droeser, P. Zajac, C. Fimognari, G.C. Spagnoli, G. Iezzi, Induction of hypoxia and necrosis in multicellular tumor spheroids is associated with resistance to chemotherapy treatment, Oncotarget, 8 (2017) 1725-1736.

[94] K.M. McMahon, M. Volpato, H. Chi, P. Musiwaro, K. Poterlowicz, Y. Peng, A.J. Scally, L.H. Patterson, R.M. Phillips, C.W. Sutton, Characterization of Changes in the Proteome in Different Regions of 3D Multicell Tumor Spheroids, Journal of Proteome Research, 11 (2012) 2863-2875.

[95] J. Laurent, C. Frongia, M. Cazales, O. Mondesert, B. Ducommun, V. Lobjois, Multicellular tumor spheroid models to explore cell cycle checkpoints in 3D, BMC cancer, 13 (2013) 73.

[96] Y. Imamura, T. Mukohara, Y. Shimono, Y. Funakoshi, N. Chayahara, M. Toyoda, N. Kiyota, S. Takao, S. Kono, T. Nakatsura, Comparison of 2D-and 3D-culture models as drug-testing platforms in breast cancer, Oncology Reports, 33 (2015) 1837-1843.

[97] C. Wigerup, S. Påhlman, D. Bexell, Therapeutic targeting of hypoxia and hypoxia-inducible factors in cancer, Pharmacology & Therapeutics, 164 (2016) 152-169.

[98] M. Wartenberg, F.C. Ling, M. Müschen, F. Klein, H. Acker, M. Gassmann, K. Petrat, V. Pütz, J. Hescheler, H. Sauer, Regulation of the multidrug resistance transporter P-

glycoprotein in multicellular tumor spheroids by hypoxia-inducible factor-1 and reactive oxygen species, The FASEB Journal, 17 (2003) 503-505.

[99] M. Wartenberg, E. Hoffmann, H. Schwindt, F. Grünheck, J. Petros, J.R.S. Arnold, J. Hescheler, H. Sauer, Reactive oxygen species-linked regulation of the multidrug resistance transporter P-glycoprotein in Nox-1 overexpressing prostate tumor spheroids, FEBS Letters, 579 (2005) 4541-4549.

[100] H.R. Mellor, R. Callaghan, Accumulation and distribution of doxorubicin in tumour spheroids: the influence of acidity and expression of P-glycoprotein, Cancer Chemotherapy and Pharmacology, 68 (2011) 1179-1190.

[101] S. Khoei, B. Goliaei, A. Neshasteh-Riz, A. Deizadji, The role of heat shock protein 70 in the thermoresistance of prostate cancer cell line spheroids, FEBS Letters, 561 (2004) 144-148.

[102] S. Khouei, G.R. Fazeli, A. Amerizadeh, D. Eslimi, B. Goliaei, Elimination of Enhanced Thermal Resistance of Spheroid Culture Model of Prostate Carcinoma Cell Line by Inhibitors of Hsp70 Induction, Cell Journal, 12 (2010) 105-112.

[103] A.S. Song, A.M. Najjar, K.R. Diller, Thermally Induced Apoptosis, Necrosis, and Heat Shock Protein Expression in Three-Dimensional Culture, Journal of Biomechanical Engineering, 136 (2014) 071006.

[104] S.C. Brüningk, I. Rivens, C. Box, U. Oelfke, G. Ter Haar, 3D tumour spheroids for the prediction of the effects of radiation and hyperthermia treatments, Scientific Reports, 10 (2020) 1653.

[105] S.S. Han, Z.Y. Li, J.Y. Zhu, K. Han, Z.Y. Zeng, W. Hong, W.X. Li, H.Z. Jia, Y. Liu, R.X. Zhuo, Dual-pH Sensitive Charge-Reversal Polypeptide Micelles for Tumor-Triggered Targeting Uptake and Nuclear Drug Delivery, Small, 11 (2015) 2543-2554.

[106] M. Bhagat, S. Halligan, S. Sofou, Nanocarriers to Solid Tumors: Considerations on Tumor Penetration and Exposure of Tumor Cells to Therapeutic Agents, Current Pharmaceutical Biotechnology, 13 (2012) 1306-1316.

[107] T.T. Goodman, P.L. Olive, S.H. Pun, Increased nanoparticle penetration in collagenase-treated multicellular spheroids, International Journal of Nanomedicine, 2 (2007) 265-274.

[108] E.C. Costa, V.M. Gaspar, J.G. Marques, P. Coutinho, I.J. Correia, Evaluation of Nanoparticle Uptake in Co-Culture Cancer Models, PLoS One, 8 (2013) e70072.

[109] O. Trédan, C.M. Galmarini, K. Patel, I.F. Tannock, Drug Resistance and the Solid Tumor Microenvironment, Journal of the National Cancer Institute, 99 (2007) 1441-1454.

[110] C. Box, S.J. Rogers, M. Mendiola, S.A. Eccles, Tumour-microenvironmental interactions: paths to progression and targets for treatment, in: Seminars in cancer biology, Elsevier, 2010, pp. 128-138.

[111] M.J. Lamberti, M. Rettel, J. Krijgsveld, V.A. Rivarola, N.B.R. Vittar, Secretome profiling of heterotypic spheroids suggests a role of fibroblasts in HIF-1 pathway modulation and colorectal cancer photodynamic resistance, Cellular Oncology, 42 (2019) 173-196.

[112] C.E. Vorwald, S. Joshee, J.K. Leach, Spatial localization of endothelial cells in heterotypic spheroids influences Notch signaling, Journal of Molecular Medicine, 98 (2020) 425-435.

[113] C. Pais-Silva, D. de Melo-Diogo, I.J. Correia, IR780-loaded TPGS-TOS micelles for breast cancer photodynamic therapy, European Journal of Pharmaceutics and Biopharmaceutics, 113 (2017) 108-117.

[114] A.S. Nunes, E.C. Costa, A.S. Barros, D. de Melo-Diogo, I.J. Correia, Establishment of 2D Cell Cultures Derived From 3D MCF-7 Spheroids Displaying a Doxorubicin Resistant Profile, Biotechnology Journal, 14 (2019) 1800268.

[115] E. Blanco, H. Shen, M. Ferrari, Principles of nanoparticle design for overcoming biological barriers to drug delivery, Nature Biotechnology, 33 (2015) 941-951.

[116] G.Y. Liu, L.P. Lv, C.J. Chen, X.F. Hu, J. Ji, Biocompatible Poly (d, l-lactide)-block-Poly (2-methacryloyloxyethylphosphorylcholine) Micelles for Drug Delivery, Macromolecular Chemistry and Physics, 212 (2011) 643-651.

[117] F. Ji, H. Sun, Z. Qin, E. Zhang, J. Cui, J. Wang, S. Li, F. Yao, Engineering Polyzwitterion and Polydopamine Decorated Doxorubicin-Loaded Mesoporous Silica Nanoparticles as a pH-Sensitive Drug Delivery, Polymers, 10 (2018) 326.

[118] T. Mizuhara, K. Saha, D.F. Moyano, C.S. Kim, B. Yan, Y.K. Kim, V.M. Rotello, Acylsulfonamide-Functionalized Zwitterionic Gold Nanoparticles for Enhanced Cellular Uptake at Tumor pH, Angewandte Chemie International Edition, 54 (2015) 6567-6570.

[119] C. Zhu, D. Huo, Q. Chen, J. Xue, S. Shen, Y. Xia, A Eutectic Mixture of Natural Fatty Acids Can Serve as the Gating Material for Near-Infrared-Triggered Drug Release, Advanced Materials, 29 (2017) 1703702.

[120] H. Lian, J. Wu, Y. Hu, H. Guo, Self-assembled albumin nanoparticles for combination therapy in prostate cancer, International Journal of Nanomedicine, 12 (2017) 7777-7787.

[121] Y. Li, M. Kröger, W.K. Liu, Shape effect in cellular uptake of PEGylated nanoparticles: comparison between sphere, rod, cube and disk, Nanoscale, 7 (2015) 16631-16646.

[122] I.-L. Lu, T.-I. Liu, H.-C. Lin, S.-H. Chang, C.-L. Lo, W.-H. Chiang, H.-C. Chiu, IR780-loaded zwitterionic polymeric nanoparticles with acidity-induced agglomeration for enhanced tumor retention, European Polymer Journal, 122 (2020) 109400.

[123] Y.-C. Chen, W.-T. Chiu, C. Chang, P.-C. Wu, T.-Y. Tu, H.-P. Lin, H.-C. Chang, Chemo-photothermal effects of doxorubicin/silica–carbon hollow spheres on liver cancer, RSC Advances, 8 (2018) 36775-36784.

[124] G. Chen, B. Ma, Y. Wang, R. Xie, C. Li, K. Dou, S. Gong, CuS-based Theranostic Micelles for NIR-Controlled Combination Chemotherapy and Photothermal Therapy and Photoacoustic Imaging, ACS Applied Materials & Interfaces, 9 (2017) 41700-41711.

[125] H. Lu, M.H. Stenzel, Multicellular Tumor Spheroids (MCTS) as a 3D in Vitro Evaluation Tool of Nanoparticles, Small, 14 (2018) 1702858.

[126] Y.-L. Su, K.-T. Chen, Y.-C. Sheu, S.-Y. Sung, R.-S. Hsu, C.-S. Chiang, S.-H. Hu, The Penetrated Delivery of Drug and Energy to Tumors by Lipo-Graphene Nanosponges for Photolytic Therapy, ACS Nano, 10 (2016) 9420-9433.